Dispersive and resonant properties of finite one-dimensional photonic band gap structures

Bowden, C., Scalora, Michael, Bloemer, Mark, Sibilia, Concita, D'Aguanno, Giuseppe, et al.

C. M. Bowden, Michael Scalora, Mark J. Bloemer, Concita Sibilia, Giuseppe D'Aguanno, Marco Centini, Mario Bertolotti, "Dispersive and resonant properties of finite one-dimensional photonic band gap structures," Proc. SPIE 10299, Novel Materials and Crystal Growth Techniques for Nonlinear Optical Devices: A Critical Review, 1029903 (23 June 2000); doi: 10.1117/12.419797

SPIE.

Event: Symposium on High-Power Lasers and Applications, 2000, San Jose, CA, United States

Dispersive and resonant properties of finite, one-dimensional photonic band gap structures

C. M. Bowden*, M. Scalora*+, M. J. Bloemer*, C. Sibilia**,
G. D'Aguanno***, M. Centini*** and M. Bertolotti**

*U. S. Army Aviation and Missile Command,
Redstone Arsenal, Alabama 35898
U. S. A.
**Dipatimento di Energetica, Universita di Roma
Italy
+Time Domain Corp., Huntsville, Alabama 35806
U. S. A.

*Tel: (256) 876-2650, Fax: (256) 955-7216
cmbowden@ws.redstone.army.mil

PREFACE

The report is a review of work one-dimensional photonic band gap (PBG) materials, carried out by the Quantum Optics Group at the US Army Aviation and Missile Command during the past few years. This work has benefited from national and international collaborations between academic, industrial, and governmental research organizations. The research effort has benefited from a multifaceted approach that combined innovative, theoretical methods with fabrication techniques in order to address the physics of structures of finite length, i.e., the description of spatio-temporal linear and nonlinear dynamics and boundary conditions. In this work we will review what we consider three major breakthroughs: (a) the discovery of transparent metals; (b) discovery of critical phase matching conditions in PBG structures for second harmonic and nonlinear frequency conversion; (c) development of a PBG true time delay device.

Our report addresses linear and nonlinear wave propagation in PBG materials, one-dimensional structures in particular. Most investigators generally address two and three-dimensional structures. We choose one-dimensional systems because in the past

Novel Materials and Crystal Growth Techniques for Nonlinear Optical Devices; A Critical Review,
edited by Ravindra B. Lal, Proc. of SPIE Vol. 10299 (Vol. CR77), 1029903 · © (2000) 2017 SPIE
CCC code: 0277-786X/17/$18 · doi: 10.1117/12.419797

they have proven to be quite challenging and have pointed the way to the new physical phenomena that are the subject of this report. In addition, one-dimensional systems can be used as a blueprint for higher dimensional structures, where the work is necessarily much more computationally intensive, and the physics much less transparent as a result.

BRIEF SUMMARY OF THE SECTIONS

Highlighted in this report are three significant technological accomplishments related to photonic band gap (PBG) structures; development of a new transparent conducting film, discovery of the phase matching conditions in PBGs to achieve efficient up and down-conversion of laser radiation, and a next generation optical true time delay device for applications to phased array LIDAR and RADAR.

Transparent Conductors:

Transparent conducting films have a multitude of uses including sensor protection, electrodes for flat panel displays, antennas embedded in windshields, rf mitigation, and thermal energy management. At the present time, the most widely used transparent conductor is Indium Tin Oxide (ITO). ITO is satisfactory for some applications but is limited by several features, most notable are the high resistivity of ITO films (5-100 ohms/sq.), high deposition temperature for quality films (300-400 degrees centigrade), and fixed transparency waveband (500-1200 nm).

We have developed a completely new approach to transparent conductors based on laminated metal-dielectric photonic band gap structures. The conducting PBG films consist of alternating layers of silver and magnesium fluoride. By a resonant tunneling process, photons are able to tunnel through the metal layers with extremely low loss. In one case, we experimentally demonstrated a film having a transmittance 17,000 times larger than the transmittance through single silver film containing the same amount of silver.

The key feature of the metal-dielectric PBGs compared with ITO is that metals have electrical conductivities 3 orders of magnitude larger than ITO. We have fabricated metal-dielectric PBGs with the following properties: sheet resistivty of 0.2ohms/sq., deposition of the films on a room temperature substrate, and a tunable transparency window which is dependent on the thickness of the metal and dielectric layers. These

films can have transmission windows with >80% transmittance. The center wavelength and width of the window are adjustable.

Frequency Doubling of Laser Radiation:

While many new lasers have been developed over the past 30 years that span a broad spectrum of wavelengths, there still remain laser frequencies which cannot be attained. This is especially true for short wavelength lasers in the blue and UV region and also in the IR regions. In order to reach new wavelengths, nonlinear crystals have been developed for laser frequency conversion. For efficient conversion, the pump laser and the newly generated wavelength must propagate with the same phase velocity in the crystal. This is a severe problem since all materials have some amount of dispersion. The traditional method to accomplish this "phase matching" is by angle tuning a birefringent crystal. Angle tuning is satisfactory, but puts stringent limits on the number of materials that are allowed. For example, the newly developed nonlinear polymers are not suitable because of small non-uniformities in the films.

A newer technique called quasi-phase matching eases some of these restrictions. In quasi-phase matching, the domains of the crystal are inverted at every coherence length in order to counteract the dispersion of the films. This has opened a wide range of possibilities for new materials that can be poled with strong electric fields to invert the crystal domains.

Our research has lead to a significant improvement over conventional phase matching and quasi-phase matching. It does not require angle tuning of a birefringent crystal, nor does it require periodic poling; all that is needed is a small modulation of the refractive index along the direction of propagation. An example of an index modulation would be a waveguide grating as in a fiber Bragg grating, or a multilayer stack of thin films as in traditional optics coatings. The index modulation causes changes in the velocity of the propagation of the electromagnetic wave. PBGs can accomplish this new type of anomalous phase matching. This opens the possibility to nearly all materials without the constraints of poling or angle tuning.

While the this type of phase matching is a breakthrough in itself, other properties of the dynamics of electromagnetic wave propagation in PBGs provide further significance to the achievement. At wavelengths near the band edge in PBGs, electromagnetic pulse propagates very slowly. The slow propagation velocity allows the peak power of the pump beam to build up an order of magnitude compared with the free

space peak power. In addition, the slow velocity provides longer interaction times for the conversion process, in essence, the crystal has a much longer optical path length than its physical length. (This fact is exploited in our true time delay device discussed in the next section). The net result is that the conversion efficiency is increased by orders of magnitude compared with a perfectly phase-matched device.

True Time Delay Device:

As mentioned above, electromagnetic pulses propagate very slowly through a photonic crystal at frequencies near the photonic band edge. This slowing down of electromagnetic radiation is important for the optical control of microwaves for applications in phased array radars. In this past year we have developed a major improvement in the delay by moving away from band edge frequencies and operating at frequencies near a defect mode in the crystal. The added advantage of operating at a defect state as opposed to a band edge state is that the pulse becomes localized in the crystal and it becomes possible to use the electro-optic effect to achieve high speed tuning of the delay.

A sample has been fabricated in GaAs/AlGaAs/AlAs that has been properly doped to apply a field across the defect region. According to theoretical models which were proven correct in our first device, the effective index of refraction of the sample will be tunable from 3-300. This slows the speed of light to a factor of 200 times slower than in free space. This is a record reduction in speed for an optical pulse in a solid in a linear system. Because the device is extremely small, 12 microns thick and 0.1mm by 0.1mm in area, the electro-optic switching speed is in the GHz range.

The high speed switching in conjunction with large tuning of the effective index of refraction constitutes a major improvement in the currrent technology of delay lines. Most schemes rely on an optical switch connected to fibers of various lengths or a single fiber with several Bragg gratings along the length of the fiber. Optical switches are extremely sensitive to fabrication tolerances and for the most part, have been dropped in favor of fiber Bragg gratings. However, delay lines based on Bragg gratings require tunable lasers that are expensive and have response times on the order of milliseconds.

I. TRANSPARENT METALS

(a) Introduction

In recent years, advances in photonics technology have generated a trend toward the integration of electronic and photonic devices. Photonic devices offer an array of advantages over conventional electronic devices. For example, they can provide enhanced speed of operation, reduced size, robustness to temperature fluctuations and other environmental changes, increased lifetime, and the ability to handle high repetition rates. These structures can be made of semiconductor materials, ordinary dielectrics, or a combination of semiconductors and dielectrics materials.

The intense theoretical and experimental investigations of these structures in recent years, of photonic band-gap (PBG) structures in particular [1-5], is evidence of the widely recognized potential that these new materials offer. In this regard, we cite the cases of the photonic band-edge nonlinear optical limiter and switch [6], the nonlinear optical diode [7], a high-gain, second-harmonic generation device [8], and the band-edge delay line [9]. These optical devices, whose operating principles are based entirely on the physics of the photonic band edge, are all extremely compact in nature (only a few microns in length). Many of these devices have electronic analogs.

For simplicity, substances are usually characterized by the degree to which they conduct electricity. Hence a distinction is made between good conductors (such as metals), insulators (such as glasses), and semiconductors (such as gallium arsenide). Under the right conditions, semiconductors may display properties common to both metals and insulators. The propagation of light inside these substances strongly depends on their conductive properties. Metals are highly reflective at nearly all frequencies of interest, from long radio waves to short-wavelength ultraviolet light. Some dielectric materials may be transparent across the visible spectrum (a slab of window glass, for example).

Metals are routinely used for radiation shielding purposes. On the other hand, dielectric or semiconductor materials are used in integrated-circuit environments because they allow the unimpeded propagation of light with minimal losses. Therefore, it would be desirable to have access to a substance that under the right conditions displays the properties of metals and dielectric materials at the same: a transparent metallic structure.

(b) Generic Photonic Band Gap Structures

In one dimension, a photonic band-gap material is usually composed of

alternating high and low index layers. We schematically depict the structure just described in Figure 1. Each layer can be chosen such that its width is a fraction of the size of a reference wavelength, usually one quarter of the reference wavelength. This forms a quarter-wave stack. As a consequence of this arrangement of the dielectric layers, interference effects cause some wavelengths to be transmitted, while a range of wavelengths centered about the reference wavelength, often referred to as "band-gap" wavelengths, are completely reflected. The structure depicted in Figure 1 consists of a 20-period quarter-wave alternating high and low index layers. The transmissive properties of the structure are depicted in Figure 2, where we show a plot of the transmission of light as a function of wavelength. A transmission of unity corresponds to 100% of the signal being transmitted. For illustrative purposes, we have chosen two dielectric materials: a glass, with an index $n_2 = 1.41$, and air, with an index $n_1 = 1$.

Thus, a range of wavelengths about some reference wavelength cannot propagate inside this device. On the other hand, the structure may be transparent to other wavelengths, above and below the gap. The absence of those wavelengths from the transmitted spectrum gives these structures their name, in analogy to the electronic band gap of semiconductors, where electrons having a specific range of energies cannot propagate inside a semiconductor crystal.

At wavelengths outside the photonic band gap, in a range above and below the gap, the properties of the structures are such that a series of transmission resonances and gaps are obtained, as depicted in Figure 2. The number of such resonances is equal to the

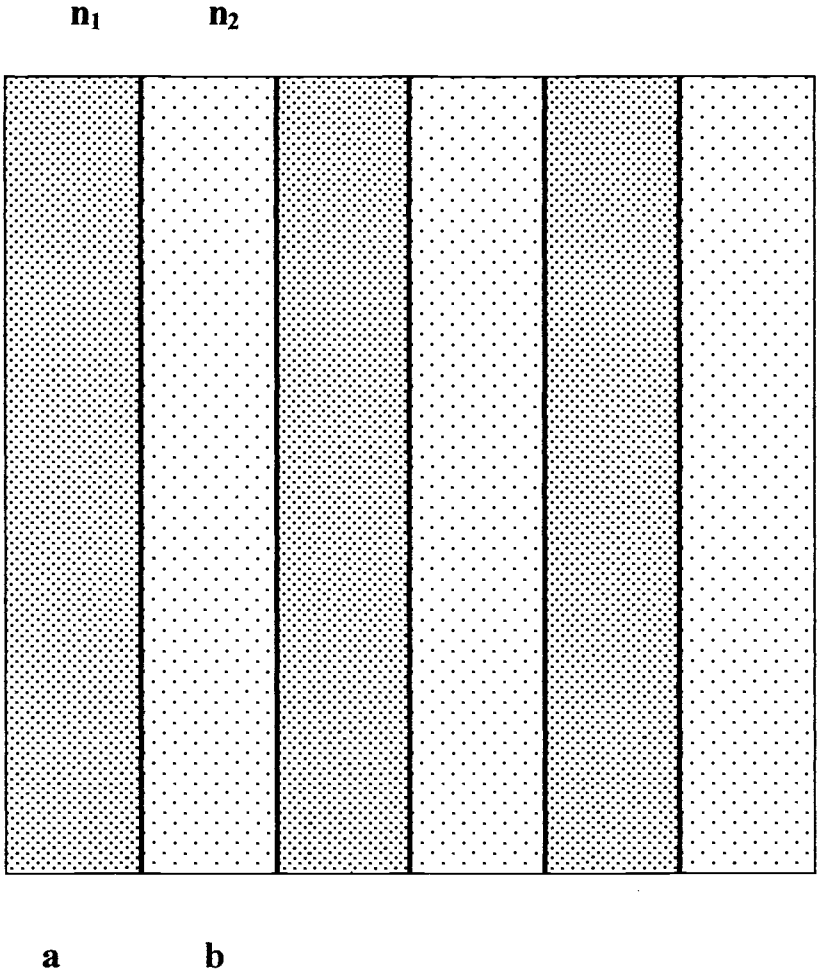

Figure 1: Generic PBG structure. The indices of refraction are n_1 and n_2 for each consecutive layer, with respective widths a and b. Each period is formed by the combination of two consecutive layers, and has width d.

number of periods that make up the structure [10]. The width of the resonances and gaps is a sensitive function of the total number of periods, the indices n_1 and n_2, and their difference $\delta n=|n_2-n_1|$, sometime referred to as index modulation depth.

Typically, the materials used in the fabrication of PBG structures are either dielectric or semiconductor substances, due to their low absorption characteristics. Metallic substances are almost exclusively used to enhance the reflective properties of dielectric or semiconductor materials by designing and incorporating within a particular device thick metallic films, such as silver, nickel, copper, aluminum or gold.

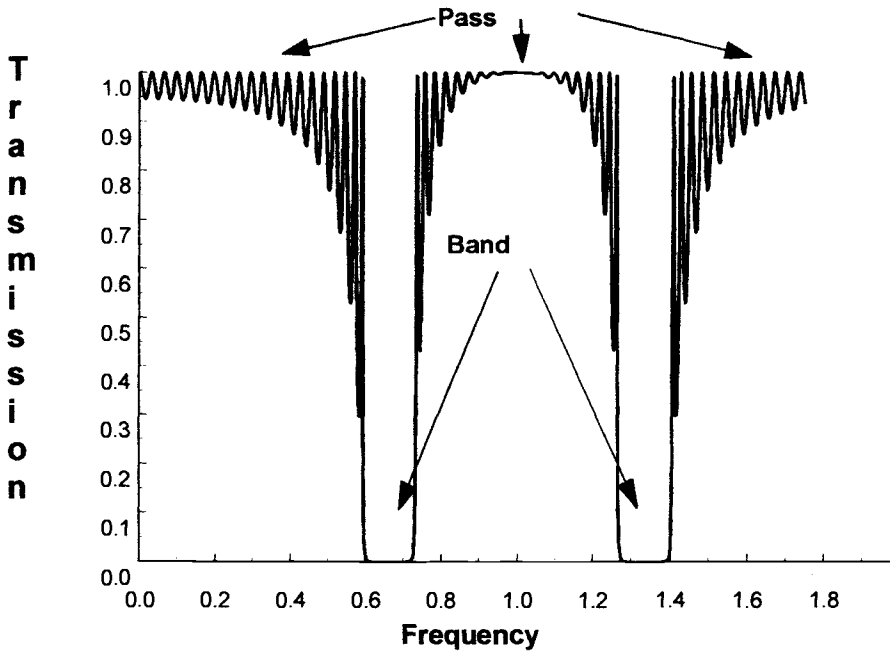

Figure 2: Transmission function for the structure depicted in Fig.(1). Note the frequency pass bands and band gaps.

(c) Metallic Photonic Band Gap Structures

Given the generic PBG structures described in the previous section, our goal now is to replace one of the dielectric layers with a metal layer. Other work on one-

dimensional PBG structures shows that the reflectivity of metallic structures can be enhanced with respect to bulk if the metal is arranged to form a periodic structure [16]. In reference [16], for example, a 256 aluminum and glass periodic structure was designed so that the reflection from such a structure increased when compared to bulk aluminum from 96% to approximately 98% for a narrow frequency range. Each metal film was assumed to be approximately 2.5 nanometers in thickness, less than the skin depth of aluminum. Even if a 256-period structure could be realized with aluminum or other metals, such a structure would be opaque to electromagnetic waves of all wavelengths, as calculations show. The traditional method to enhance the reflectivity of a metal is to grow a dielectric distributed Bragg reflector on the metal film. The combined dielectric DBR and metal film provide enhanced reflectivity with just a few periods [17]. Therefore, it is possible to make better mirrors by introducing and combining metals with periodic PBG structures. However, we attempt to answer what we believe is a fundamentally more difficult question: is it possible to propagate light through thick metal films, and render them transparent to visible light? This means focusing specifically on the transmissive properties of PBG structures where thick metal films may be a major component.

To our knowledge, no previous work addresses the possibility of rendering a layered, metallic structure transparent to visible light, while at the same time maintaining its reflective properties for low-frequency radiation. The reason for this is that it is generally thought that either an increase in thickness, or the presence of additional metal layers, can drastically reduce the transmission of visible light. In fact, we predict that the transmission at visible wavelengths does not change appreciably, and can be controlled more effectively, with a metallo-dielectric, periodic structures that has more than two metal layers. In addition to the transparency region, the reflective properties of the resulting structure are as good as those of a metal shield for very-low-frequency (VLF) and extremely-low-frequency (ELF) radiation.

(d) Layered Metallic Structures

The layered, metallic PBG structures that we discuss are typically composed of a metal; such as gold, silver, or copper; and a dielectric or semiconductor material. We presently use the metal silver (symbol Ag) and the glass magnesium fluoride (symbol MgF_2), as an example to illustrate the physical properties of our device and its operation.

Each metal layer may be as thin as 10 nanometers (or thinner, as long as the properties of the layer are smooth and uniform throughout). The total net thickness of Ag across each structure may be hundreds of skin depths in length. As we will see below, the thickness of the MgF_2 layers can also vary. We focus our attention on the transmissive properties of a structure composed of several alternating Ag and MgF_2 layers deposited on a glass substrate. Our calculations were performed using the matrix transfer method [20], and the beam propagation method [21]. We calculated the transmission spectra as a function of a number of parameters that included the incident wavelength or frequency, the number of layers, and layer thickness. We used the data for the refractive index and the absorption of these materials, as measured and reported in the book by Palik [19]. We modeled the substrate with a type of glass whose index of refraction is approximately 1.5 for a wide range of incident wavelengths. The purpose of the substrate is, in general, to hold the material components in place, and its exact physical properties may also vary.

(e) Examples

As a first example, we consider a single Ag layer 40 nanometers in thickness suspended in air. We show the sample in the inset (a) of Figure 3. Our calculations show that this sample transmits 2.5% of the incident red light, 8% of green light, and about 15% of blue light (Figure 3, red line). Thus, this film relects most of the visible light incident on it. However, if we now imagine we could separate the original 40 nanometer film into 4 films each about 10 nanometers in thickness, and space each Ag layer with approximately 110 nanometers of MgF_2 [Figure 3, inset (b)] then the total transmission of visible light increases to an average of 70% (Figure 3, blue line).

As another example, a silver film 200 nanometers in thickness [Figure 4, inset (a)] is completely opaque to nearly all frequencies. We calculate that only 10^{-7} of the incident visible light will be transmitted. (Figure 4, red line). On the other hand, if we once again separate the original Ag film into 20 layers of Silver, each about 10 nanometers thick, and place a thickness of about 140 nanometers of MgF_2 as the intervening medium

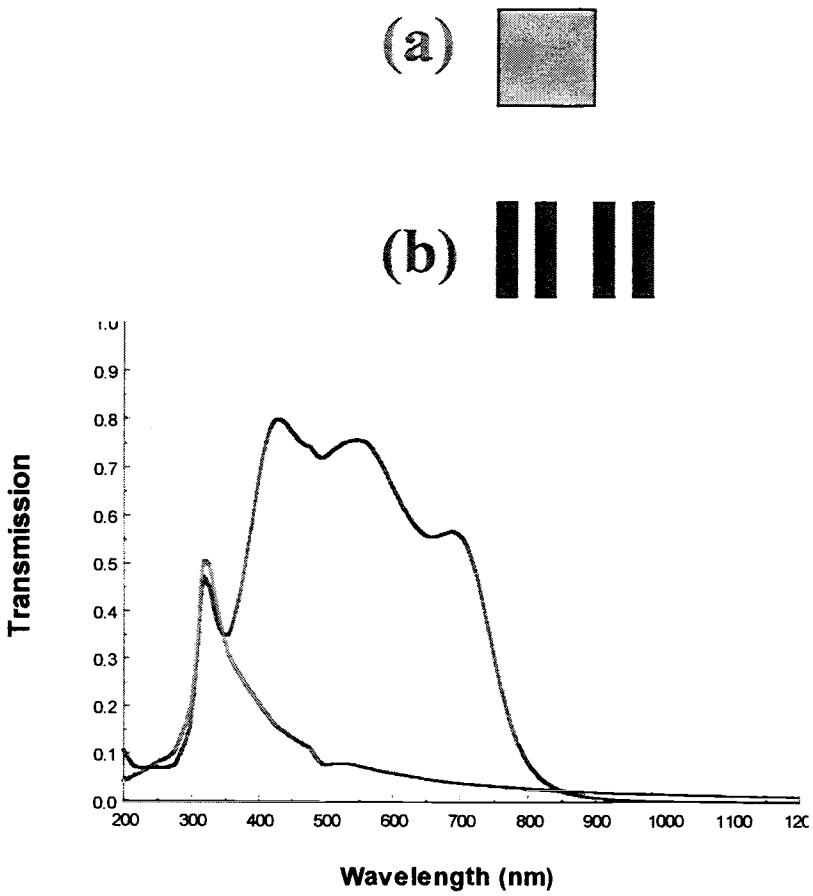

Figure 3: Transmission vs. wavelength for a 4-period PBG sample (solid line) and a solid Silver film 40 nm thick (dotted line). Silver layers are 10 nm thick, while the MgF_2 layers are 120 nm thick. Inset: bulk (a) and pbg (b) samples.

between the silver layers [Figure 4, inset (b)], then the average transmission in the visible range of frequencies increases to an average of 50% (Figure 4, blue line), or about seven orders of magnitude better transmission than for the single 200-nm Silver film case. At the same time, the periodicity of the structure also ensures better suppression of the

transmitted light at longer wavelengths, and also for part of the ultraviolet frequency range.

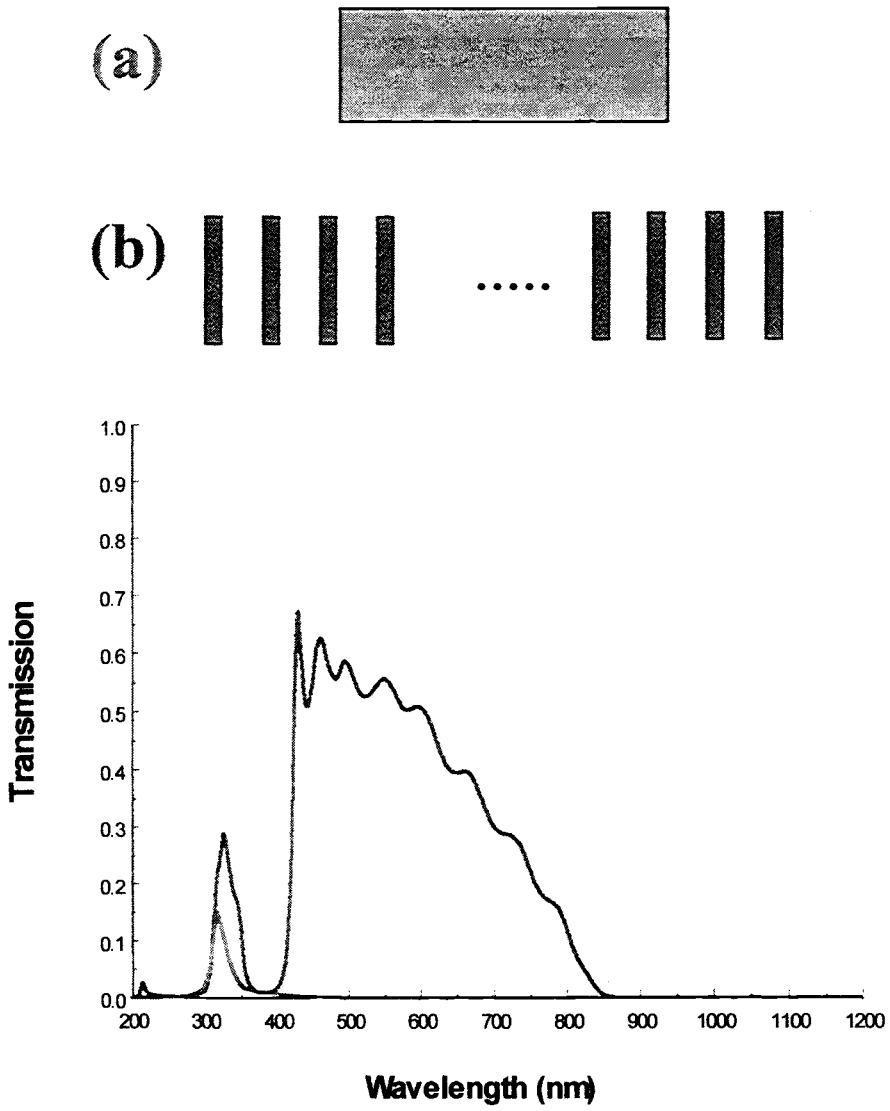

Figure 4: Same as Figure 3, except that for the PBG sample MgF_2 layers are 140 nm thick, and the solid Silver film is 200 nm thick.

Generally speaking, adding more Ag and MgF_2 periods to the structure causes a decrease in the transmitted light intensity. For example, although we do not show this, our calculations suggest that a 40-period Ag and MgF_2 structure, where each Silver layer is 10 nanometers in thickness, and each MgF_2 layer is approximately 200 nanometers thick, causes the average transmission in the visible range to decrease to approximately 10%. At the same time, the transmission at all longer wavelengths, beginning in the near infrared at about 800 nanometers, is well below 10^{-20} for this example. This is an extremely high degree of isolation, with essentially zero transmission.

Our calculations also suggest that decreasing the number of periods and increasing metal layer thickness leads to much the same results. Therefore, in the examples that follow, we will use structures that contain three periods, but where the thickness of each metal layer is approximately 30 nanometers. As we have illustrated in Figs.3-5 this is considered a thick metal film at visible wavelengths; ordinarily, it would be considered counterintuitive to add more, and perhaps thicker metal layers in order to improve the transmissive properties of the structure.

In Figure 5, we show a structure composed of a glass substrate, and a three-period, Ag and MgF_2 metallic PBG structure (Figure 5a). We compare the properties of this structure to those of a single thick metallic film that contains the same amount of silver on the same substrate (Figure 5b). Each silver layer in Figure 5a is taken to be 30 nanometers thick. MgF_2 layers are about 150 nanometers thick.

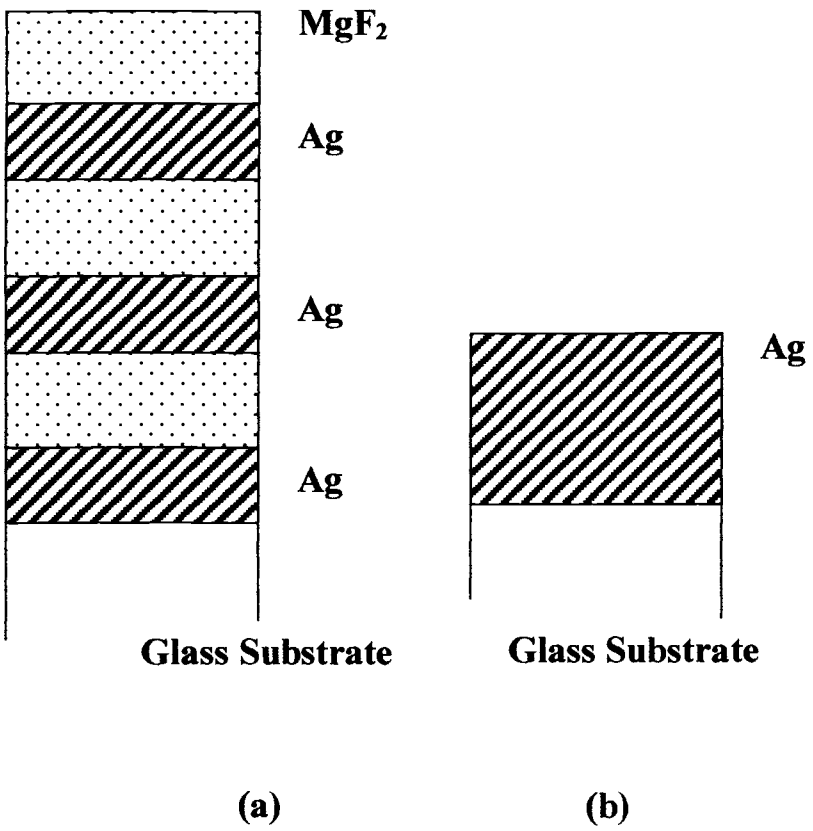

Figure 5: Schematic representation of three-period PBG, where each metal layer is 30 nm thick (a); and 90-nanometer thick silver film (b) on substrate.

In Figure 6, we show the results of the calculated transmission of light as a function of incident wavelength for the two structures shown in Figure 5. We note that the transmission from the solid metal film (red line) is approximately 10^{-3} in the visible range of wavelengths. On the other hand, the maximum transmission through the periodic structure is nearly 50% of the incident radiation, or four orders of magnitude greater compared to the solid metal film, with a peak in the green, around 520 nanometers. This transmissive range extends over a good portion of the visible range. As in the Figures 3-4, a transmission resonance also appears at about 320 nanometers, in the ultraviolet

frequency range. This transparency is not due to the periodicity of the structure, since it can be identified for both samples shown in Figure 5. It is an intrinsic property of silver, which becomes slightly transparent at the plasmon resonance, in the ultraviolet range, provided metal films are not too thick.

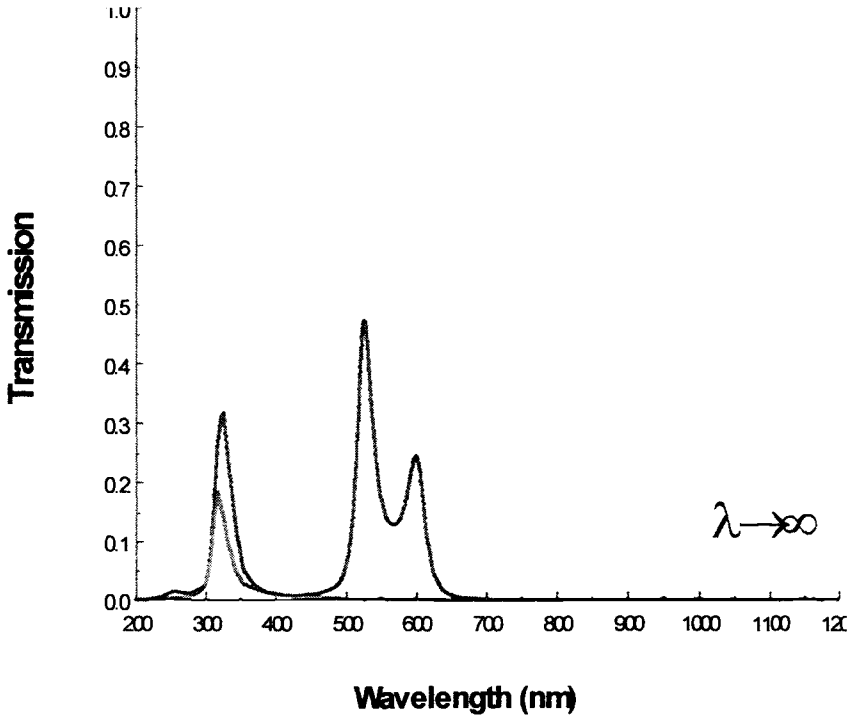

Figure 6. Transmission vs wavelength for a Ag/MgF_2 PBG (blue line) and the continuous silver film (red line) shown schematically in Figure 5.

(f) The Drude Model and the Low Frequency Limit

We would now like to extend our predictions to include low frequency, Ghz radiation. This part of the spectrum is routinely used for communication purposes. The available data for most ordinary metals extends from the mid- to far-infrared frequency range, i.e., 1-30 microns. Therefore, we use the Drude model [8] for metals in order to numerically calculate (at very low frequencies) the characteristic transmission spectra for

our periodic PBG structures. The model provides a good theoretical representation of the dielectric constant (or index of refraction and absorption characteristics) for most metals, including silver, for a range of frequencies that includes low-frequency, radio waves and high-frequency, near-ultraviolet light. The dielectric function can easily be derived, and it can be written as [16,18]

$\varepsilon(\omega) = 1 - [\omega^2_p /(\omega^2 + \imath\gamma\,\omega)]$,

where ω_p is the plasma frequency, and γ is the damping coefficient. We choose to depict our results as a function of frequency so that it will be simple to extrapolate to zero frequency (or infinite wavelength) without ambiguity. For silver, we use ω_p= 7.2 eV, and γ=0.05 eV, which are typical values for metals such as copper, gold, silver and aluminum.

In Figure 7, we plot the transmission versus frequency for our three-period metallic PBG depicted in Figure 5. The figure shows that the transmission of light is suppressed for all frequencies up to the visible range, where a maximum of about 50% is transmitted through the sample; this agrees well with the results of Figure 6. The Drude model is quite simplistic in that it cannot predict the transparency region found at about 320 nanometers. In Figure 7, this would occur slightly to the right of visible range, around $4x10^{14}$ Hz, where the silver plasmon resonance occurs. We see that a band-gap characterizes a good portion of the ultraviolet frequency range, which is also suppressed. More importantly, the small-frequency range depicted in Figure 7 includes all communication frequency bands, microwave, and infrared light. The calculation also suggests that in the limit of zero-frequency, i.e., ELF and VLF radiation, the transmission is suppressed down to levels better than 1 part in 10000 of the incident values. Therefore, the results in Figure 7 represent the theoretical realization of what we referred to as a transparent metallic structure: it is transparent in the visible range, and it acts like a good metal reflector at all lower frequencies.

We note that this particular realization of transparent metals is not unique, in that different metals and dielectric (or semiconductor) thickness may be used. For example, our calculations suggest that it is also possible to use a combination of two or more metals, or two or more types of dielectric or semiconductor materials within the same structure, without any significant departure from the basic characteristics that we have described. The frequency range where light is transmitted can be changed by either increasing or decreasing the thickness of the magnesium fluoride layers. Increasing (decreasing) the thickness of the dielectric material cause a shift of the band structure

toward longer (shorter) wavelengths. So a structure can be fabricated such that a band-gap characterizes the visible range. By the same token, it may be possible to make better far-ultraviolet and soft x-ray reflectors by judiciously choosing the contents and the periodicity of the structure.

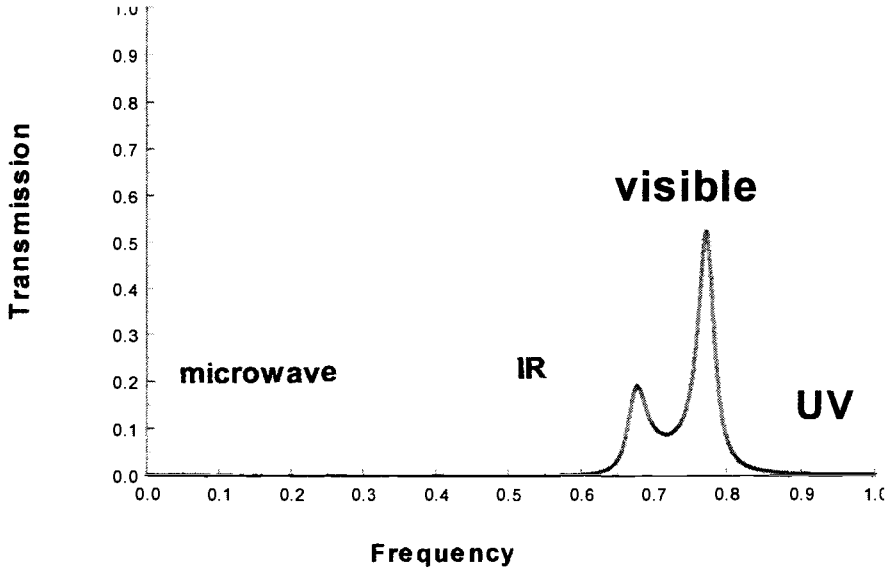

Figure 7: Drude model calculation of transmission vs frequency. Theory predicts a transparency region at visible wavelengths, a band gap at ultraviolet frequencies, and nearly complete rejection of all lower frequencies, including infrared, microwave, and radio waves.

(g) Metallic Fabry-Perot Cavity

In order to provide some physical insight into our results, we consider the following system: two silver films 40 nanometers in thickness, separated by a distance L, to form a Fabry-Perot cavity with metallic mirrors of finite thickness. We depict this simple structure in the inset of Figure 8. We assume an incident wavelength of approximately 1000 nm, such that the index of refraction is approximately n = 0.2 + i7 [19]. We let the field be incident form the left. Assuming continuous boundary conditions on the field and its derivatives, we solve for the transmission coefficient through this structure as a function of L. The calculation is equivalent to solving a double barrier problem with five regions of interest, and can easily be carried out

analytically. We plot the results in Figure 8. The figure suggests that a transmission resonance occurs whenever film separation is almost a multiple of the $\lambda/2$, as expected. However, it is not exactly a multiple of $\lambda/2$ due to the finite thickness of the metal walls.

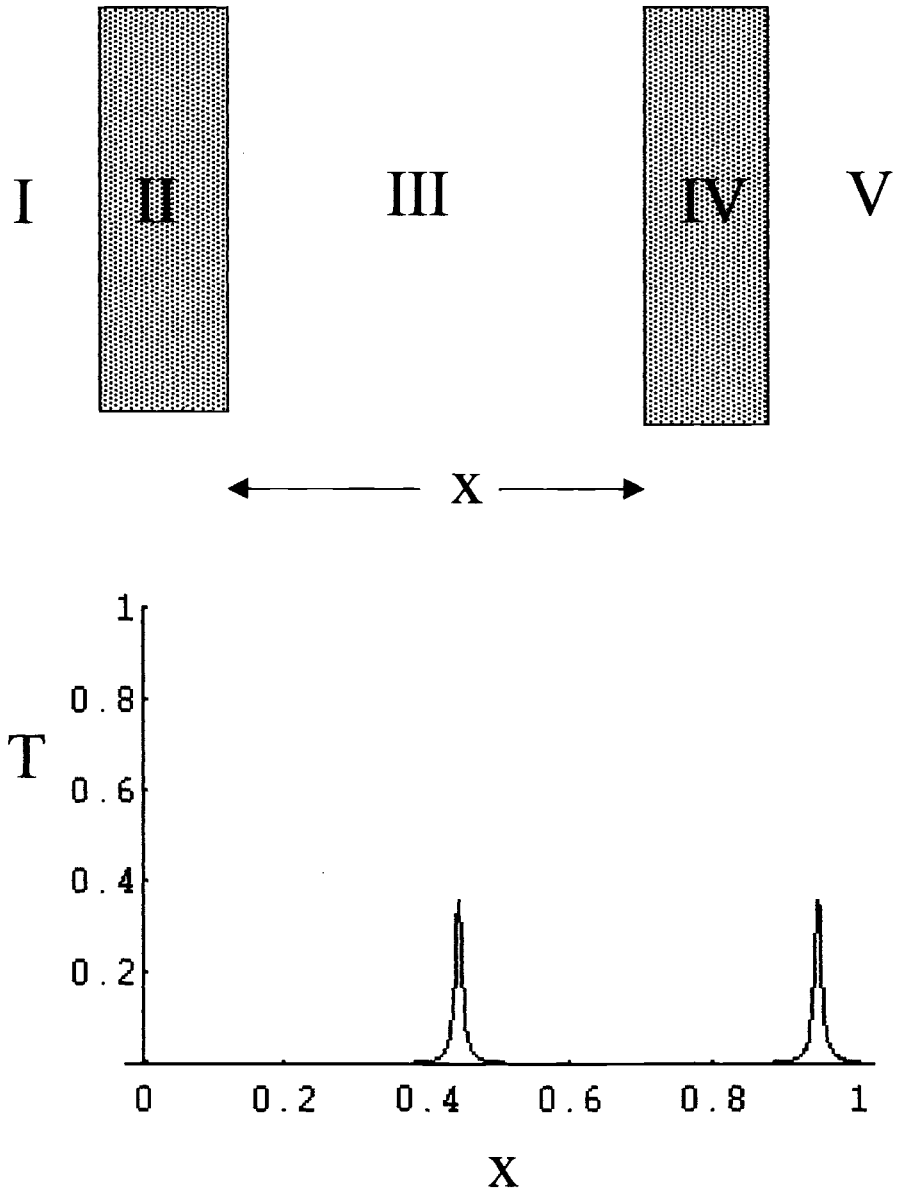

Figure 8: Transmission coefficient vs cavity length calculated for a simple metallic Fabry-Perot cavity having 40-nanometer thick metal walls. A transmission resonance occurs when the condition $nL=2\lambda$ is approximately satisfied, as expected. Adding more periods generates the band structure, with as many resonances within a pass band as there are periods. Inset: schematic representation of the structure, and the regions where we seek solutions for the wave equation.

It was surprising, however, to find that the transmission from a compound structure that contains 80 nm of silver is still a remarkable 40% of the incident value.

The effect that we observe in our simulations amounts to resonance enhanced tunneling of electromagnetic waves. The introduction of a second metal layer, and hence additional boundary conditions, can create the right set of circumstances that lead to a kind of induced transparency such that the effective absorption coefficient inside the metal is also suppressed. This suggests that boundary conditions cause a significant redefinition of skin depth for metals, and as a consequence its meaning cannot be taken at face value.

(h) Experimental Results

We now describe the experimental results. The metallo-dielectric (MD) PBG samples were grown in a standard thermal evaporation chamber having dual sources. The base pressure of the chamber was $2x10^{-6}$torr. The films were deposited on a glass microscope slide (Corning 2947 glass) situated 50cm from the resistively heated sources. The substrate was not temperature controlled. A movable shield, positioned 1cm below the substrates but not obscuring the crystal thickness monitor allowed impurities to burn off, the deposition rate to stabilize, and simultaneous fabrication of samples having a different number of periods without breaking vacuum. The first layer of the periodic stack, silver, was deposited at a rate of ~0.3nm/sec. The MgF_2 layers were deposited at a rate of ~0.5nm/sec. These slow deposition rates provided good control and repeatability of the layer thickness. Based on *in situ* measurements of the film thickness by the crystal thickness monitor and subsequent profilometric measurements on a DekTac II, the thickness control on each layer of the sample (at a given point on the sample) was ~0.3nm for the Ag and ~0.5nm for the MgF_2. The variation of the film thickness across the surface of the sample was 12% for the silver and <2% for the MgF_2 over a 6cm distance.

Sample 1 consisted of 2.5 periods of Ag(38nm)/ MgF_2(233nm) for a total Ag thickness of 114nm; Sample 2 was 2.5 periods of Ag(26nm)/ MgF_2 (140nm) with a total Ag thickness of 78nm. A third sample was nearly identical to Sample 2: having an extra period, i.e., 3.5 periods of Ag(23nm)/ MgF_2 (140nm) for a total Ag thickness of 92nm. Samples 2 and 3 were grown side by side in the evaporation chamber, which resulted in Sample 3 having slightly thinner Ag layers.

Adding a final layer of MgF_2 to the structure, for an integral number of periods, has very little effect on the transmittance spectra. However, it is possible to improve the transmittance of the pass band by ~15% if a final layer of MgF_2, having ~1/2 the thickness of the internal MgF_2 layers, is applied.

As mentioned earlier the choice of MgF_2 for the dielectric is not crucial to the optical performance of the MD-PBG sample. The main parameters of the dielectric, aside from the mechanical properties of adhesion and durability, are the refractive index of each layer and the thickness which will determine the location of the pass band and the gap and the angular dependence of the band structure. As the angle of incidence increases from the normal, the band structure blue shifts. This occurs in spite of the fact that the optical path through each layer increases with angle: the extra path for the beam reflected at the air-surface interface increases at a faster rate, causing the blue shift, and a path difference decrease with increasing angle of incidence. For a high index dielectric, the shift in the band structure with angle is much less pronounced than for a low index dielectric due to the smaller angle of refraction of the transmitted beam.

The normal incidence transmittance spectrum was measured in a Shimadzu UV-260 spectrophotometer. The transmittance of the 1mm thick glass substrate was measured separately: it was found to be nearly 90% from 340-900nm, 78% at 320nm, and 50% at 300nm. The experimental transmittance data of the samples have been corrected for the absorption in the substrate and the small reflection loss at the substrate-air interface.

In computing the theoretical transmittance spectra, the optical constants for Ag and MgF_2 were taken from Ref.14. For the Corning 2947 glass substrates, prism coupling was used to measure the index at several wavelengths from 488nm to 1310nm. Since the dispersion of the glass was slight, <1%, we used a constant value of 1.51 to simulate the glass index. The absorption of the glass below 340nm was neglected in the calculations. The thicknesses of the layers measured by a profilometer were equal to the theoretical values (within the uncertainty of the thickness measurement which was +/-2%).

For reference, Figure 9 shows the theoretical transmittance for a single film of silver on a glass substrate. The thickness corresponds to the total amount of silver contained in each of the three samples, i.e. 114nm, 78nm, and 92nm, respectively. The transmission resonance at 320nm is near the plasma frequency for silver. The

transmittance of silver drops sharply for shorter wavelengths due to the onset of inter-band transitions from the d-band to empty conduction band (p-band) states near the Fermi level. The artificial shoulders in transmittance at 370nm are the juncture between the measured optical constants of silver from two different experimental groups compiled in Ref.14. In the visible wavelength region, the transmittance of a 100nm thick silver film is $\sim 1 \times 10^{-3}$.

Figure 10 shows the experimental and theoretical transmittance through Sample 1, which contains a total of 114nm of silver. The stop band extends throughout most of the visible and has prominent transmission resonances at the band edges. The gap width is 50% of the center frequency. Looking through the sample in bright sunlight, the sample transmits a beautiful violet color at normal incidence and red at off-normal angles.

A typical dielectric/dielectric PBG (DD-PBG) has highly transmissive pass bands that extend between all stop bands, down to dc frequencies. The unusual band structure for MD-PBGs, compared to DD-PBG, results from two properties of metals: the high reflectivity at frequencies below the plasma frequency and the large dispersion in the extinction coefficient. The real part of the complex index of refraction for silver is ~0.15 from 400nm to 900nm while the extinction coefficient varies from 2 to 6 over the same wavelength interval. Therefore, the long wavelength pass band shuts down after the second transmission resonance at 810nm because the optical potential is rapidly increasing with the extinction coefficient. The short wavelength pass band also shuts down after the second transmission resonance because of low reflectivity and absorption due to interband transitions. The transmission resonance at 320nm is a property of bulk silver as depicted is Fig.9.

The most interesting and perhaps the most important feature of the MD-PBGs is the existence of highly transmissive pass bands. At 755nm, the transmittance of Sample

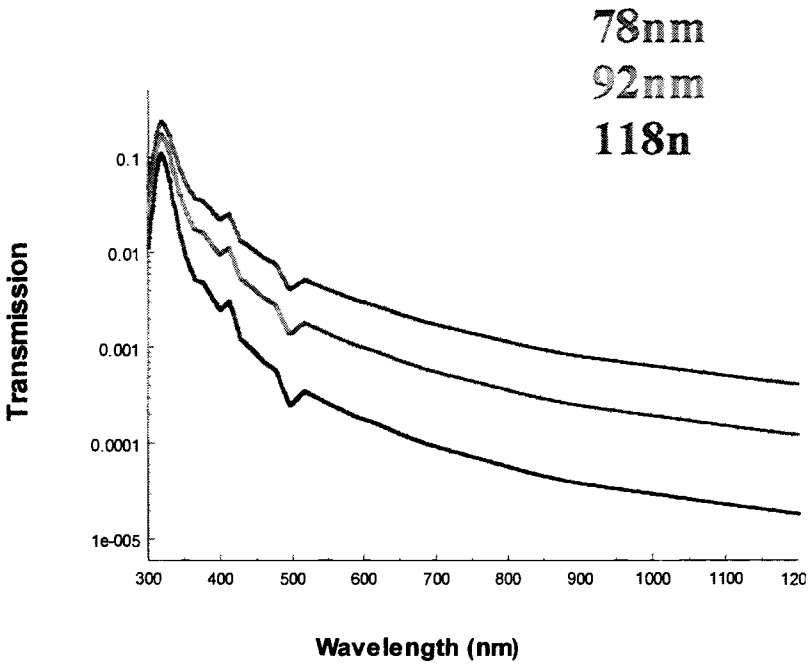

Figure 9: Theoretical transmittance of a 78nm, 92nm, and 114nm thick silver film on glass.

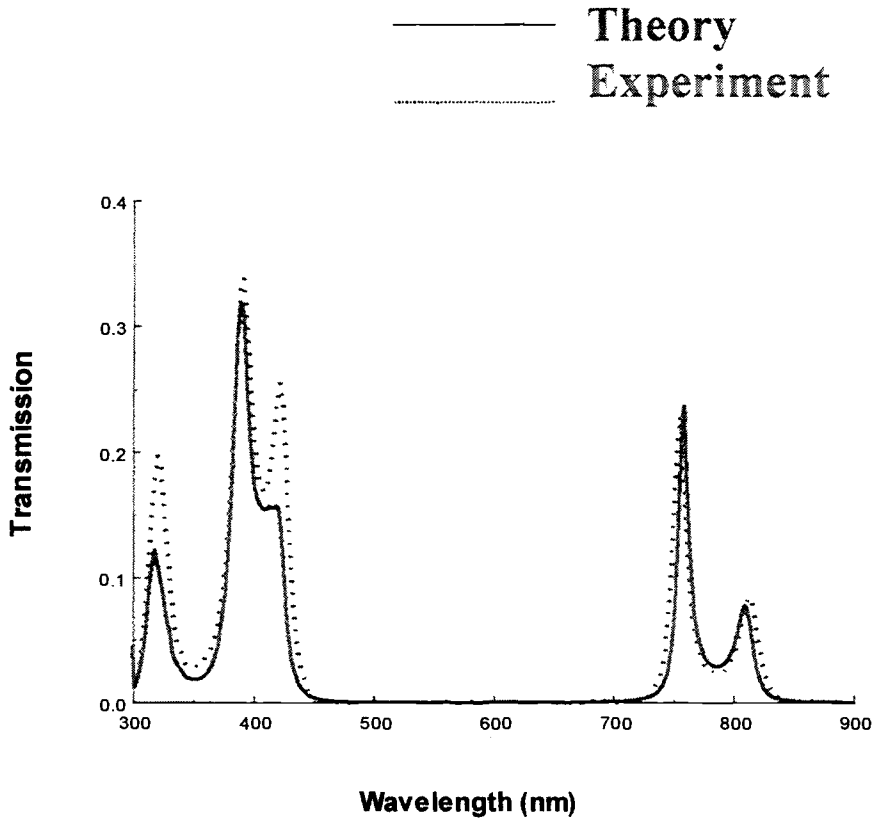

Figure 10: Experimental and theoretical transmittance of a MD-PBG containing 2.5 periods of Ag(38nm)/ MgF_2(233nm). The stop band spans nearly the entire visible spectrum. The transmission resonance at 320nm is a property of bulk silver.

1 is 23%, which is 3,000 times larger than expected for a single silver film 114nm thick (this factor may be slightly exaggerated in real samples as a result of pinhole defects and other imperfections in the silver film). In addition to highly transmissive pass bands are stop bands which are deeper than for the corresponding thickness of a single silver film. At 570nm, for example, the experimental transmittance of Sample 1 was $1.5x10^{-4}$; this should be compared with the theoretical value of $2.2x10^{-4}$ for a single silver film of equivalent thickness. However, the theoretical transmittance of Sample 1 is $7.4x10^{-5}$, which is a factor of two less than what was actually measured.

Although Fabry-Perot transmission resonances using two partially transmitting silver mirrors are common in spectroscopy and other areas, what is surprising is that broad, highly transmissive, pass bands can be achieved in MD-PBGs and that the overall transmission in the pass band may actually increase as more silver is deposited. This feature is illustrated in Samples 2 and 3. Figure 11 shows the theoretical and experimental transmittance of 2.5 periods of Ag/ MgF_2; Figure 12 shows the transmittance of a 3.5 period MD-PBG (note that the long wavelength pass band has been shifted to the visible by using only 140nm of MgF_2 instead of the 233nm used in Sample 1). The 3.5 period sample contains 14nm more silver than the sample with 2.5 periods; yet, the overall transmittance in the pass band is greater for the 3.5 period sample. The view through this sample is also very interesting: at normal and near normal incidence, the sample is essentially transparent with a light greenish tint. Based on the bulk properties of a single silver film, the transmittance should be reduced by a factor of 3 due to an additional 14nm of Ag (see Fig.9). This is an example of the enhancement of resonant tunneling, as a result of boundary conditions and small optical path inside the metal.

The transmittance spectrum of the pass band can be designed by adjusting the thicknesses of the Ag and the number of periods [9]. A pass band from 440nm to 850nm can be obtained by using a 5 period MD-PBG having 10nm thick Ag layers, and still maintain >50% transmittance through most of the pass band. Adding more periods has the tendency to flatten the oscillations in the pass band, and steepen the skirts at the edges of the band. For applications where the UV transmission resonance at 330nm is undesirable, replacing one or two Ag layers of the MD-PBG with Au (which has a

slightly lower plasma frequency than Ag) will block the UV without changing the properties of the pass band.

The microwave properties of the MD-PBG were measured with an HP 8510B Network Analyzer, 8514B S-Parameter Test Set, and a 8360 Synthesized Sweeper. Since the skin depth ($d_{skin} = \lambda/4\pi k$, where k is the extinction coefficient and λ is the free space wavelength) of metals at microwave frequencies is on the order of microns, there was some question whether a MD-PBG containing only 0.1μm of Ag would actually block the radiation as predicted in Ref.9 and as discussed above. A baseline sweep from 8-20GHz was taken with a rectangular waveguide having a cut-off frequency of ~6GHz. The waveguide was then opened, Sample 2 inserted, and the transmittance recorded with the 2 sections of the waveguide separated by the thickness of the sample. A similar measurement was recorded with the waveguide blocked by a 1/2mm thick sheet of copper to determine the noise floor for the apparatus. The measurement showed that Sample 2, with only 78nm of silver, blocked the microwaves as well as the thick copper.

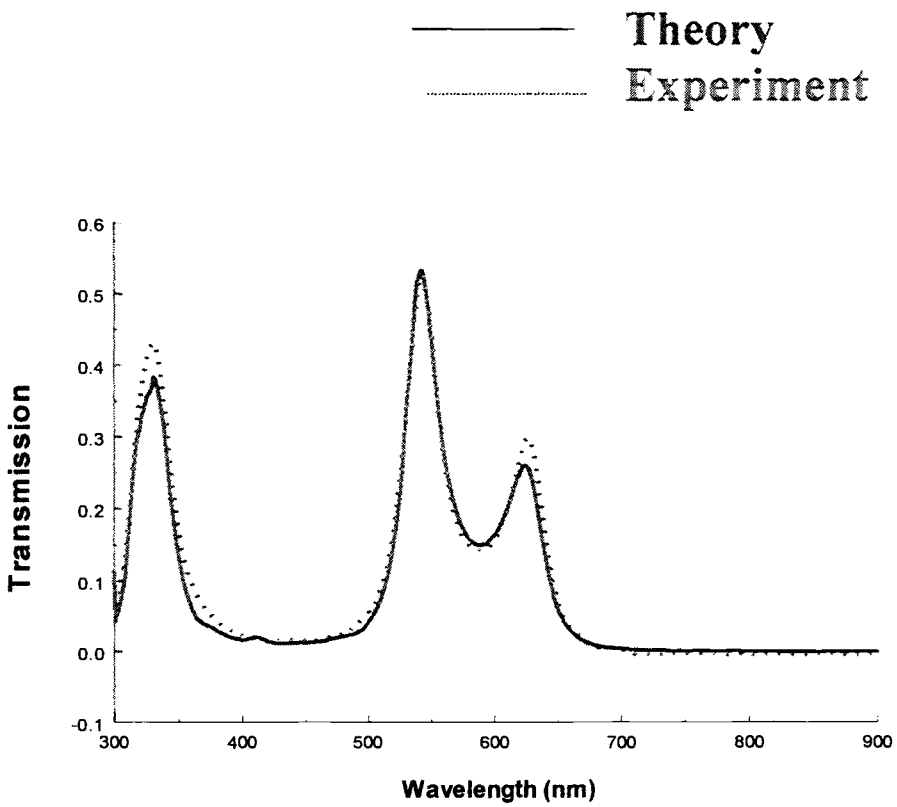

Figure 11: Experimental and theoretical transmittance of a MD-PBG containing 2.5 periods of Ag(27nm)/ MgF_2(155nm). The transmission resonance at 330nm is a property of bulk Ag. The lowest energy pass band is in the visible as a result of the thinner MgF_2 layers. The next pass band is predicted at 235nm with a transmittance of <10%.

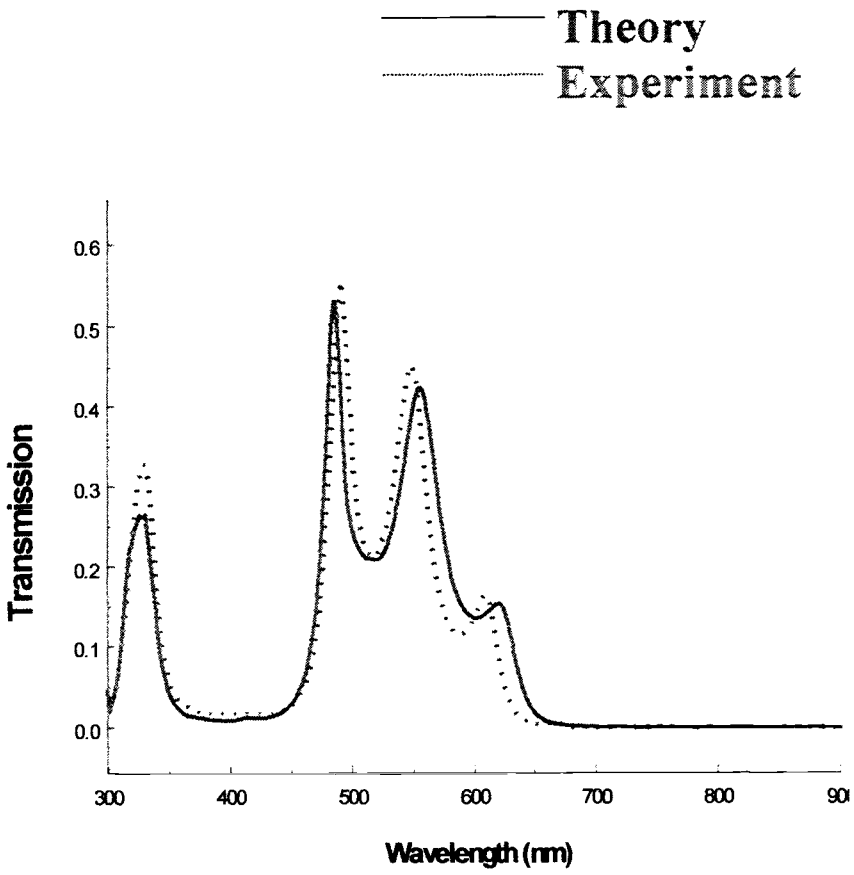

Figure 12: Experimental and theoretical transmittance of Sample 3, a MD-PBG containing 3.5 periods of Ag(23nm)/ MgF_2(140nm). The y-scale is the same as in Fig.3. The overall transmittance in the pass band is larger than for the sample of Fig.3 even though an extra period has been deposited (14nm more Ag). The transmittance at the band edge remains at 55% as in Sample 2.

sheet down to the noise floor limit of -35dB. The glass substrate had little effect on the microwaves other than a small reflection loss. Measured losses resulting from a 1mm gap in the waveguide was only ~3dB. These microwave results indicate that although the skin depth in metals at microwave frequencies is large relative to optical frequencies, the potential barrier at microwave frequencies allows only a small fraction of the radiation to actually penetrate into the metal.

These optical and microwave experiments demonstrate the essential features of transparent metals based on the unique band structure of 1-dimensional MD-PBGs; a highly transmissive, tunable pass band having deep stop bands on either side. The long wavelength stop band extends from optical frequencies to static fields. Pass bands at frequencies above the plasma frequency are highly attenuated by interband absorption.

Applications for transparent metals include laser safety glasses, heat reflecting windows, display windows on rf equipment, and transparent conductors. The figure of merit for a transparent conductor is $F_{TC} = T/R_S$, where T is the optical transmittance and R_S is the electrical sheet resistance. The standard transparent conductor, indium tin oxide (ITO), has an optical transmittance of ~80%, but has resistivities three orders of magnitude larger than metals. This makes the figure of merit for transparent metals more than two orders of magnitude better than for the best conducting oxide films. In addition, low resistance MD-PBGs provide faster switching speeds than ITO based devices. The MD-PBGs are ideal for electrodes on light emitting polymer displays where tailoring of the emission spectrum is required for proper color.

Finally, we simply point out that our discovery amounts to the fact that light can be transmitted through thick, periodic, metallic structures, and by controlling the thickness of the dielectric or semiconductor sandwiched between the metal films, as well as the thickness of each metal film, the transparency regions can be tuned. Just as significantly, the structure acts like a good metal reflector for all lower frequencies. In our discussion, we have highlighted the importance of boundary conditions and optical path. One cannot overstate their importance when interference effects dominate the dynamics, as in the case of a periodic, PBG structure. Even more so in the case of a metallo-dielectric PBG structures, which by virtue of their induced transparency and shielding abilities can lead to new types of devices.

REFERENCES

[1] E. Yablonovitch, *Phys. Rev. Lett.* **58**, 2169 (1987).

[2] *Development and Applications of Photonic Band-gap Materials,* edited by C. M. Bowden, J. P. Dowling, and H. O. Everitt, J. Opt. Soc. Am. B **10**, 279-413 (1993), special issue.

[3] *Principles and Applications of Photonic Bandgap Structures,* edited by G. Kurizki and J. W. Haus, J. Mod. Opt. **41**, 171–404 (1994), special issue.

[4] *Photonic Crystals,* J. D. Joannopoulos, R. D. Mead, and J. N. Winn, Princeton University Press, Princeton, 1995.

[5] J. He and M. Cada, IEEE J. Quant. Elec. **27**, 1182 (1991); N. D. Sankey, D. F. Prelewitz, and T. G. Brown, Appl. Phys. Lett. **60**, 1427 (1992); J. He, M. Cada, and M. A. Dupertuis, J. Appl. Phys. **63**, 866 (1993), and references therein; W. Chen and D. L. Mills, Phys. Rev. Lett. **58**, 2169 (1987); C. M. de Sterke and J. Sipe, Phys. Rev. A**38**, 5149 (1988); D. N. Christodoulis and R. I. Joseph, Phys. Rev. Lett. **62**, 1746 (1989); A. Kozhekin and G. Kurizki, Phys. Rev. Lett. **74**, 5020 (1995).

[6] M. Scalora, J. P. Dowling, C. M. Bowden, and M. J. Bloemer, Physical Review Letters **73** 1368, (1994).

[7] M. Scalora, J. P. Dowling, M.J. Bloemer, and C. M. Bowden, Journal of Applied Physics **76**, 2023 (1994).

[8] M. Scalora, M.J. Bloemer, A.S. Manka, J.P. Dowling, R. Viswanathan, J.W. Haus, and C.M. Bowden, Physical Review A, (1997).

[9] M. Scalora, R. J. Flynn, S. B. Reinhardt, R. L. Fork, M. D. Tocci, M. J. Bloemer, C. M. Bowden, H. S. Ledbetter, J. M. Bendickson, J. P. Dowling, and R. P. Leavitt, Physical Review E **54**, 1078R (1996).

[10] J. M. Bendickson, J. P. Dowling, and M. Scalora, Physical Review E 53 , 4107 (1996).

[11] V. Kuzmiak and A. A. Maradudin, Phys. Rev. B **55**, 7427 (1997); V. Kuzmiak, A. A. Maradudin, and F. Pincemin, Phys. Rev. B **50**, 16835 (1994); A. R. McGurn and A. A. Maradudin, Phys. Rev. B **48**, 17576 (1993).

[12] D. F. Sievenpiper, M. E. Sickmiller, and E. Yablonovitch, Phys. Rev. Lett. 76, 2480 (1996).

[13] K. A. McIntosh, L. J. Mahoney, K. M. Molvar, O. B. McMahon, S. Verghese,

M. Rothschild, and E. R. Brown, Appl. Phys. Lett. **70**, 2937 (1997); E. R. Brown and O. B. McMahon, Appl. Phys. Lett. **67**, 2138 (1995).

[14] E. Ozbay and B. Temelkuran, M. Sigalas, G. Tuttle, C. M. Soukoulis, and K. M. Ho, Appl. Phys. Lett. **69**, 3797 (1996); M. M. Sigalas, C. T. Chan, K. M. Ho, and C. M. Soukoulis, Phys. Rev. B **52**, 11744 (1995); J. S. McCalmont, M. M. Sigalas, G. Tuttle, K.-M. Ho, and C. M. Soukolis, Appl. Phys. Lett. **68**, 2759 (1996).

[15] Toshio Suzuki and Paul K. L. Yu, Opt. Lett. **20**, 2520 (1995).

[16] A.J. Ward, J.B. Pendry, and W.J. Stewart, Journal Physics Condens. Matter **7**, 2217 (1995).

[17] *Optical Thin Film,* J. D. Rancourt, SPIE Optical Engineering Press, 1996.

[18] *Classical electromagnetic radiation,* J. B. Marion, Academic Press, 1965.

[19] *Handbook of Optical Constants of Solids*, E.D. Palik editor, Academic Press, 1985.

[20] *Modern Optics*, G.R. Fowles, Dover Publications, second edition, 1975.

[21] M. Scalora and M.E. Crenshaw, Optics Communications 108, 191 (1994); M. Scalora, J. P. Dowling, A. S. Manka, C. M. Bowden, and J. W. Haus, Physical Review A **52**, 726 (1995).

II. NONLINEAR FREQUENCY CONVERSION: SECOND HARMONIC GENERATION

Previous investigations of nonlinear optical behavior in large-index modulation, one-dimensional PBG structures by other authors have focused on $\chi^{(3)}$ processes such as optical switching and gap-soliton propagation. In two recent publications [5],and [6], we pointed out that there may be advantages in pursuing nonlinear frequency conversion in a PBG structure. Our results generally indicated that the enhancement mechanism that we predicted can lead to frequency up- (or down-) conversion rates nearly three orders of magnitude better than conversion rates achieved with ordinary quasi phase matched (QPM) materials. QMP refers to the case where the fields are phase-matched to the same index of refraction.

In a PBG case, the geometrical properties and the periodicity of the photonic "crystal" can act to significantly modify the density of electromagnetic field modes near the band edge, interaction times, group velocity, and linear phase matching thus facilitating the emission of the SH signal at a much enhanced rate. More importantly perhaps, this means that current fabrication issues that arise in ordinary quasi–phase–matched structures can be avoided altogether by utilizing current technology for deposition of semiconductor or dielectric thin films.

The reason for the enhancement of gain in these structures can be understood from the following arguments. In quasi-phase-matched structures, a minimization of the phase difference between the waves is desirable in order to avoid a phase mismatch in the CW case. This is typically achieved by poling the active material — which is *uniform* in its composition and contains *no linear index discontinuities* — in such a way that the nonlinear coefficient only alternates sign in the longitudinal direction, every few tens of microns. Here, our approach departs significantly from convention. We rely on the unusually strong confinement of *both* the pump and the SH signal that occurs near the photonic band edges, where the density of electromagnetic field modes is large, and the group velocity is low. The field amplitude may be enhanced over bulk values by one order of magnitude or more, strong pump and SH mode overlap, and a new type of linear phase matching occurs. The combination of these processes is ultimately responsible for the enhanced gain that we observe in our simulations. In what follows we will first briefly review the field. We will then focus on the new aspects of our research which

deal with newly discovered phase matching conditions in periodic structures.

In a recent publication [6] the theoretical enhancement of second harmonic generation at the band edge of a mixed quarter-half wave PBG structure was discussed . The structure was chosen so that both the pump and second harmonic fields were tuned near the first and second order band edges respectively. We found that maximum conversion efficiency was achieved by tuning the pump at the first transmission resonance of the first order gap, and by tuning the second harmonic at the second transmission resonance of the second order gap, as shown in Figure.(1). Second harmonic enhancement, which was predicted to be several orders of magnitude larger compared to an exactly phase matched bulk structure of the same length, was attributed to several factors: an increase in the mode density, and a corresponding decrease in group velocity; an increased interaction time; strong mode overlap. The novelty of the approach outlined above rests on the fact that the active material is not poled in the usual way in order to produce a phase matched device. Instead, the process relies on the linear, geometrical properties of the structure to significantly enhance second harmonic gain.

Under ordinary circumstances, efficient second harmonic generation requires some kind of phase matching condition to be satisfied, i.e., $2k(w)=k(2\omega)$. This condition clearly requires the conservation of linear momentum. In a multilayer structure, part of the field propagating in the structure is back-reflected. This process clearly does not conserve the momentum if the role of the reflecting interface is not taken into account [5]. When generation of the second harmonic field is considered, again the role of the reflecting interface must be taken into account in an even more complex way due to the presence of two forward (fundamental and SH) and two backward fields. The simple equality of phase velocity for the interacting fields is therefore not sufficient to generate momentum conservation. On the other hand, it is well known that efficient second harmonic conversion requires phase velocity matching.

For the conditions we are interested in, pulse or cw propagation near the band edge, forward and backward propagating components inside the structure can easily be of the same order of magnitude, even if ultimately there are no pump reflections from the structure. The reason for this is that the formation of a quasi-standing wave at the transmission resonance requires both forward and backward components to be present at the same time, thus raising the possibility of forward and backward generated second harmonic fields. In the case of pulses, pump reflections are guaranteed by the finite

frequency make up of the pulse, and hence total momentum is generally not a conserved quantity [5,6].

In this report, we examine how phase matching conditions are established in a periodic structure, and how this knowledge can be used for device design purposes. We will show that linear material dispersion can be combined with the geometry of the structure to achieve phase matching, that is, the equivalence of the indices of refraction at ω and 2ω. This process is to be compared and contrasted with the usual quasi phase matching process, where the nonlinear domains are inverted every coherence length to form a structure that is periodic in the nonlinear coefficient only, and where the background index is constant [7]. Therefore, we evaluate and discuss a simple method for obtaining the equivalent index of refraction (effective index) , and compare the results with the direct integration of Maxwell's equations in the time domain, using the same method and formalism discussed in ref.[6].

(a) Formalism

The simple method that we discuss is based on the evaluation of an effective refractive index for a multilayered structure, based on a formulation of the effective dispersion relation. The method is generally valid for many situations, ranging from long fiber gratings with weak periodicity, to deep gratings with high index contrast. Perhaps more importantly, periodicity is not essential. The matrix transfer method [8] allows us to construct the transmission function for any structure, namely, $t \equiv x + iy \equiv \sqrt{T}e^{i\varphi_t}$, where $\sqrt{T}$ is the transmission amplitude, $\varphi_t=\tan^{-1}(y/x)\pm m\pi$ is the total phase accumulated as light propagates through the medium. Here the integer m is uniquely defined assuming $\varphi_t(\omega)$ is a monotonically increasing function, and the condition that $m=0$ as $\omega \rightarrow 0$ is satisfied. Starting from the analogy of propagation in a homogeneous medium, we can express the total phase associated with the transmitted field as

$$\varphi_t = k(\omega)D = \frac{\omega}{c} n_{eff}(\omega) D \qquad (1)$$

where $k(\omega)$ is the effective wave vector, and n_{eff} is the effective refractive index that we attribute to the layered structure whose physical length is D.

The presence of gaps in the transmission spectrum, where the propagation of light is forbidden, suggests that the effective index of the structure should be complex. In

particular, the index should have a large imaginary component inside the gap, to allow for nearly 100% scattering losses, i.e., reflections and evanescent field modes. Thus we simply recast the transmission function as follows: first, we assume that $\sqrt{T} = |t| = e^{-\alpha D}$. This implies that an incident field of unit amplitude is "attenuated" by an amount $e^{-\alpha D}$, where $\alpha = (\omega/c)n_i$, and n_i is the imaginary component of the index. According to this picture, we write $\sqrt{T} = e^{\ln\sqrt{T}}$ and the complex transmission becomes $t = e^{\ln\sqrt{T}} e^{i\varphi_t} = e^{i\varphi} = x + iy$. Therefore,

$$i\varphi = i\varphi_t + \ln\sqrt{T} = i\left(\frac{\omega}{c}\hat{n}_{eff} D\right) \qquad (2)$$

where we still have $\varphi_t = \tan^{-1}(y/x) \pm m\pi$ as before, which allows us to rewrite Eq.(2) as:

$$\hat{n}_{eff}(\omega) = (c/\omega D)\ [\varphi_t - (i/2)\ln(x^2+y^2)\ ]. \qquad (3)$$

Eq.(3) suggests that at resonance, where $T = x^2+y^2 = 1$, the imaginary part of the index is identically zero. Inside the gap, where the transmission is small, scattering losses are expected to be high, leading to evanescent waves. We can also define the effective index as the ratio between the speed of light in vacuum and the effective phase velocity of the wave in the medium. We have $\hat{k}(\omega) = \frac{\omega}{c}\hat{n}_{eff}(\omega)$. This is the effective dispersion relation of the structure. Usually, the dispersion relation for periodic structures is obtained by applying periodic boundary conditions to the wave equation for an infinite, *periodic* structure. According to Bloch's theorem [9,10], Eqs.(1) and (2) reduce to $\cos(k(\omega)d) = 1/2\,\mathrm{Tr}[M]$, or

$$\cos(k(\omega)d) = \left[\cos\left(\frac{n_1\omega a}{c}\right)\cos\left(\frac{n_2\omega b}{c}\right) - \frac{n_1^2 + n_2^2}{2n_1n_2}\sin\left(\frac{n_1\omega a}{c}\right)\sin\left(\frac{n_2\omega b}{c}\right)\right] \qquad (4)$$

Here, M is the scattering matrix for the elementary unit cell which constitutes the periodic structure; n_1 and n_2 are the refractive indices of layers of thickness a and b respectively, and d= a+b. Equation (4), is valid only for a periodic structure with an infinite number of layers, that is, if there are no input or output interfaces. Our approach, which was developed principally for finite structures, gives results that are in complete agreement with the results of Eq.(4), provided the number of periods is large. The

validity of Eq.(3) is general because it holds for any kind of layered structure, periodic or not.

As an example, let's consider the 20-period, quarter-wave/half-wave structure, already discussed in ref.[6]-see Fig.(1). Using the matrix transfer method, we construct the transmission function $t = x + iy$, and use the results to calculate the effective index, as given by Eq.(3). The results are depicted in Fig.(1), where we plot the real (dashed line) and imaginary components (dotted line) of the effective index of refraction. We note that the real part of the index displays anomalous dispersion inside the gap. The imaginary component is small and oscillatory in the pass-bands; it attains its maximum at the center of each gap, where the transmission is a minimum. By adopting the effective index formulation we have replaced the layered structure with an effective medium of length D. Then, the transmission function for the layered structure depicted in Fig.(1) can be faithfully reconstructed using Eq.(3). This gives us a consistent physical picture of the scattering process, including the accurate predictions of group velocity, density of modes, and spontaneous emission rates [4-6,10]. More importantly, the Kramers-Kronig relations for the effective index are identically satisfied. That is, given the imaginary part of the effective index as $\mathrm{Im}(n_{eff}) = (1/2)\ln(x^2 + y^2)$, the real part of the effective index is recovered. We will discuss the details in a future publication [11].

Since we are interested in phase matching conditions, let's focus our attention on the real part of the effective index. Again with reference to [6], we find that for the simple 20-period structure the effective refractive indices have precisely the same value at the pump and second harmonic frequencies, as shown in Fig.(1). That is, the conditions for efficient SH generation reported in ref. [6] are also those that satisfy exact phase matching between the fields, i.e., $n_{eff}(\omega) = n_{eff}(2\omega) \approx 1.334$ in this case. It is evident that modifying material dispersion, number of periods, and layer thickness modifies the effective index since all these quantities modify the transmission spectrum. In this manner, structures can be designed to satisfy different criteria, third harmonic generation or frequency down-conversion, for example.

In the case of finite structures, an interesting phenomenon occurs: the dispersion relation gives rise to different effective indices of refraction for counterpropagating waves. In this effective medium picture, counter-propagating waves travel with different phase velocities *inside* the same medium. The effective forward and backward indices that we calculate are the same only for infinite structures, which are somewhat idealized

and unrealistic. In particular, we predict unusual discrepancies between the phase velocities of forward and backward propagating components, which can have significant implications in the phase-matching problem at hand. More care must be exercised when calculating the dispersion relation for the reflected field. Using symmetry considerations between LTR (left to right) and RTL (right to left) incident waves, it can be shown that

[12] $r^{-}(\omega) = -\{r^{+}(\omega)\}^{*} \dfrac{t(\omega)}{t^{*}(\omega)}$, where ± refers to LTR and RTL respectively.

Defining LTR and RTL reflection coefficients in a manner similar to the definition of the transmission coefficient on page 37, namely, $r^{-}(\omega) = \mid r \mid e^{ik^{-}(\omega)D}$ and $r^{+}(\omega) = \mid r \mid e^{ik^{+}(\omega)D}$, and by further defining $\varphi^{\pm}(\omega) = k^{\pm}(\omega)D$, it follows that

$$\tilde{\varphi}(\omega) = \varphi_t(\omega) \pm m\frac{\pi}{2}, \qquad \text{m=1,3,5,7,...} \qquad (5)$$

where $\tilde{\varphi}(\omega) = \dfrac{\varphi^{+}(\omega) + \varphi^{-}(\omega)}{2}$. Equation (5) suggests LTR and RTL phases cannot be related unambiguously, and the solution to Eq.(5) is not unique. On the other hand, Eq.(5) allows us to define an upper and a lower bound for the average phase, in the same way that an upper and a lower bound can be found for the corresponding group velocities, which can be calculated from Eq.(5) [12]. In Fig.(2-a), we plot the effective index calculated from the average phase in Eq.(5) for m=1 (dashed upper curve) and m=-1 (dotted lower curve). The solid line is the effective index for the forward propagating components. That is, the simple model can only assign an upper and a lower bound to the average effective index calculated for backward propagating waves. Suffice it to say here that our results suggest that RTL and LTR propagation cannot in general be considered separately, but that all ambiguities can be lifted by solving Maxwell's equations in the time domain, as we do below, and by calculating the effective wave vectors for waves propagating inside the PBG. As we will see, this aspect of the solution that we present is novel in the study of PBG structures.

In Fig.(2-b), we depict the effective indices upon transmission for a 2, 10, and 20-period structure, and compare with the results of dispersion relation Eq.(4). This figure makes it clear that the effective, dispersive properties of the structures are modified by the number of periods, and converge to the infinite-structure results of Eq.(4). Although we do not show this in the figure, we again point out that in the limit of a large number of periods, the upper and lower bounds on the average reflected effective indices shown in Fig.(2-a) also converge to the transmitted effective index, an indication that the effective index for forward and backward components become degenerate and indistinguishable from Eq.(4).

The results presented above were obtained by using simple arguments that follow from the application of the matrix transfer method. These results suggest that this phase mismatch may be the reason why, in this case, the forward propagating field is preferentially enhanced, as the results of ref.[6] suggest. In the limit of large number of periods, both forward and backward fields experience the same effective index, and one should then expect similar results for transmitted and reflected SHG.

To confirm these results, starting from Maxwell's equations, we have examined pulse propagation in a finite PBG structure, as described in ref.[6]. Our goal was to verify that phase velocities of counter-propagating waves inside the structure are in fact different, as predicted by our simple effective index model. In the calculation, we use a Gaussian input pulse that is approximately one picosecond in duration, and it is tuned to the first resonance near the first order band edge, at ω/ω_0=0.591 (see Fig.(1)). Pulse length is hundreds of times longer compared to the length of the structure [6], and pulse bandwidth can be considered to be much smaller than band-edge transmission resonances. In Fig.(3-a), we plot the Fourier transform $|E_\omega(k)|^2$ of the incident pump field as a function of the wave vector k when the peak of the pulse has reached the structure. In the dynamics, four components can be identified. Two correspond to free space propagation, at $\pm k_0$, i.e., portions of the pulse have been transmitted and reflected from the structure.

The other two components are transient, and they are clearly visible as long as energy lingers inside the structure. An analysis of the other two components reveals that the locations of the center of gravity of each wave packets, denoted by –k' and k'', are consistent with the values obtained using the simple effective index calculation depicted in Fig.(2-a), and indicate that indeed forward and backward components propagate with

different phase velocities. We highlight and contrast the difference between the backward propagating wave packet of Fig.(3-a) with that of Fig.(3-b), where we choose ω/ω_0=0.738, which corresponds to the high frequency band edge. In this case, Maxwell's equations clearly indicate a shift of the effective index for backward propagating waves from the higher to the lower curve of Fig.(2-a). It would have been difficult to predict this behaviour using the simple model presented above. Therefore, the solutions shown in Fig.(3) can only inspire caution when results obtained for structures of infinite length are generalized to structures of finite length, especially without the benefit of a simple verification of propagation effects in real, finite systems.

We note that the wave packets of Fig.(3) are quite broad, and in fact their widths corresponds to a range of effective refractive indices. Unlike the free space components at $\pm k_0$, the widths of the wave packets at –k' and k" are independent of incident pulse width, an effect that persists in the quasi-monochromatic wave regime. Therefore, we interpret this effect as a simple consequence of the sudden confinement of the incident wave to a space of width D, which excites a range of wave vectors such that $\delta k \cong 1/D$. To conclude this section, we note that the equations of motion have been integrated using a FFT-BPM [6], and a FDTD integration scheme that makes no approximations, both giving similar results.

Mindful of the limitations imposed by the simple model that we use, our results show that the effective index approach explains well the phase matching conditions present in periodic structures. Our calculations suggests that this is true for second and third harmonic generation, and we believe that it may be true in general for any kind of one-dimensional geometry, including quasi-periodic and random structures.

For phase matching in periodic structures, a simple connection can be made between our effective index approach and Block's phase β [4, 13] for infinite structures. While we leave the details for exposition in a future work [11], it can be shown that beginning with the phase matching condition that we find, that is $n(\omega) = n(2\omega)$, and taking advantage of the analytical expression of the transmission of a finite structure written as a function of the Bloch phase [4], then $\beta_2(2\omega)=2\beta_1(\omega)$ is satisfied for second harmonic generation, as one might expect for infinite structures. This is obviously a particular case (for periodic structures) of the more general phase matching conditions as expressed by the effective index approach .

To summarize, the effective index approach provides a unique, simple, and fast method to achieve and optimize phase matching in dispersive media via the matrix transfer method. Normal material dispersion can be overcome by proper choice of layer thicknesses. In addition to phase matching, photonic band gap structures offer several other advantages, such as increased density of modes, large field enhancements, low group velocity, and field overlap. The combination of band edge effects and phase matching through anomalous dispersion provides efficiencies orders of magnitude larger than quasi-phase-matching. These results are valid for layered structures with large index contrast, long grating structures [14] or waveguides having small index modulation depth, and structures that are not periodic. Although we have specifically addressed the lowest frequency band gaps, similar arguments apply to higher order band gaps. The advantage of using higher frequency gaps is that the periodicity of the index modulation can be on a longer length scale, which would ease fabrication tolerances for grating structures. Finally, the analogy that is usually drawn between photonic and electronic band structure brings us full circle to predict the same phenomena described above for electrons in finite, solid state nanostructures. While we cannot predict with certainty what effects can be expected for electron waves in matter, the concept is very intriguing and merits further investigation.

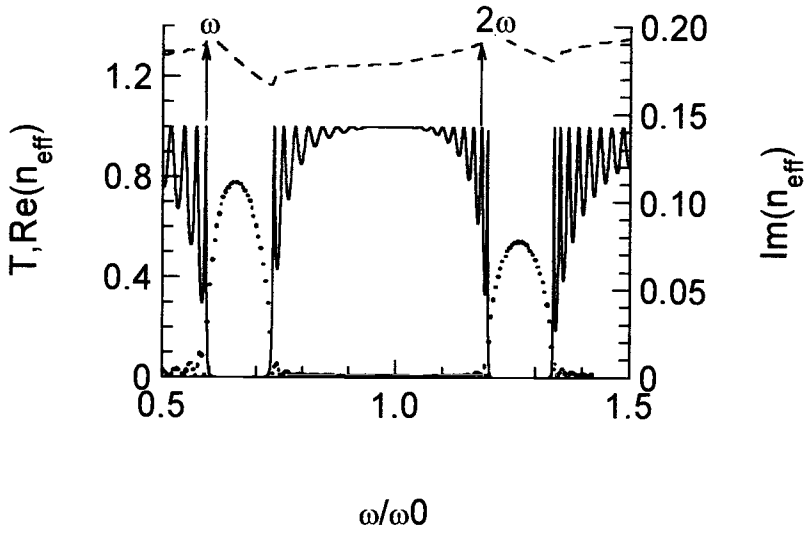

Fig.1- Transmittance and complex effective indices of a 20-period, quarter-wave/half-wave structure, with layer thicknesses a = $\lambda/(4n_1)$, b= = $\lambda/(2n_2)$, where λ is the free space wavelength. The indices of the layers are: $n_1(\omega)=n_1(2\omega)=1$; $n_2(\omega)=1.4285714$ and $n_2(\omega)=1.519$. This amount of dispersion provides good phase matching for the structure. Other values of dispersion can be phase-matched by properly adjusting layer thicknesses. Solid line: transmission spectrum. Dashed (Dotted) line: real (imaginary) part of the effective index.

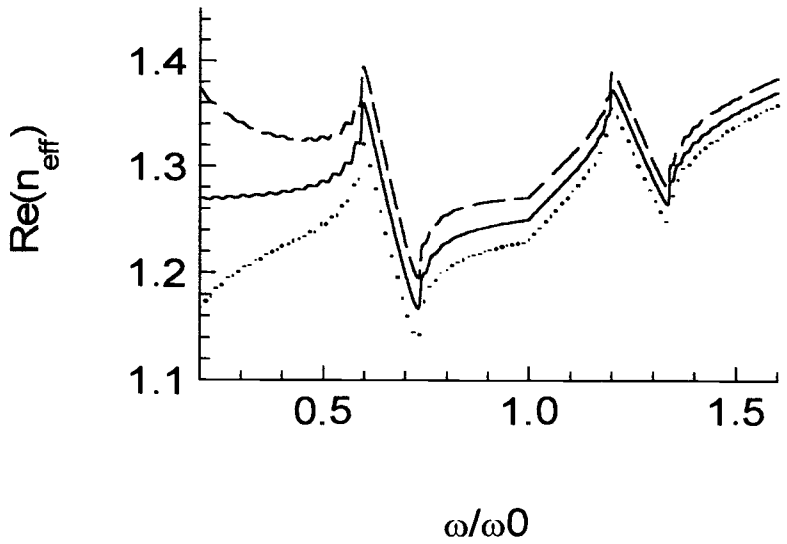

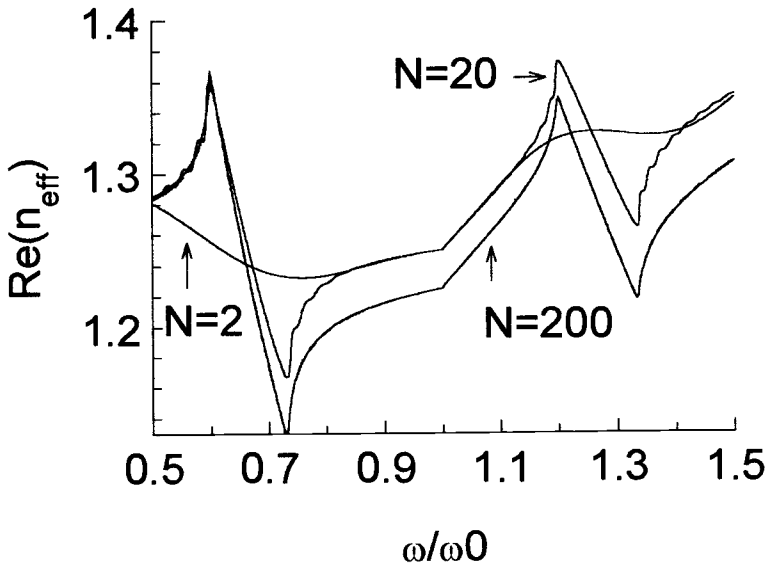

Figs.2 –For the structure described in Fig.(1). **(a)** Solid Line: real part of the corresponding effective index of refraction for forward propagation. Dashed (Dotted) : real part of average effective index of refraction for reflected components for m=1 (m=-1). **(b)** Same as Fig.(2-a), but with 2, 20, 200, and an infinite number of periods, each as indicated by the arrow. Note the dependence on N of the dispersion around the band edges.

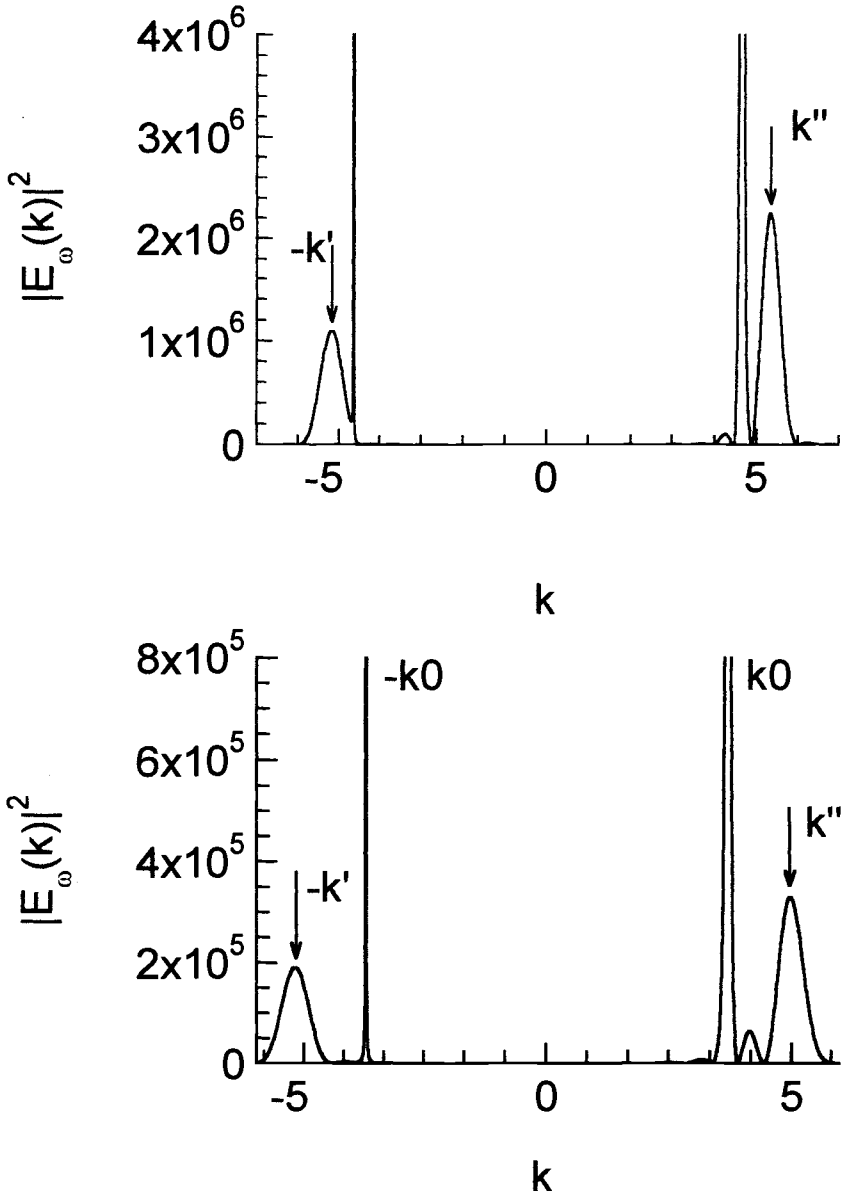

Figs.3 Fourier components for pump wave packets at a time when the peak of the pump pulse reaches the center of the structure. **(a)** For pump tuned at low frequency band edge, ω/ω_0=0.591; **(b)** the pump is tuned at the high frequency band edge, ω/ω_0=0.738. Components at $\pm k_0$ represent free space components; -k' an k'' are the carrier wave vectors inside the structure, which are transient, and correspond to the effective vectors in the effective index approach. Note the relative location of the reflected peaks with respect to the reflected free space components in both (a) and (b).

REFERENCES

1. .J.D. Joannopoulos, P.R. Villeneuve & S. Fan, Nature **386**, 143 (1997).
2. S. John, Phys. Rev. Lett. **58**, 2486 (1987).
3. E. Yablonovich and T.J. Gmitter, Phys. Rev. Lett. **67**, 2295 (1991).
4. M.Tocci, M. Scalora, M.J. Bloemer, J.P. Dowling, C.M. Bowden, Phys. Rev. A **53**, 2799 (1995); J.M. Bendickson, J.P. Dowling, M. Scalora, Phys. Rev. E **53**, 4107 (1996).
5. M. Scalora, J.P. Dowling, A. S. Manka, C. M. Bowden, and J.W. Haus, Phys. Rev. A **52**, 726 (1995).
6. M. Scalora, M. J. Bloemer, A. S. Manka, J. P. Dowling, C. M. Bowden, R. Viswanathan, and J. W. Haus, Phys. Rev. A **56**, 3166 (1997).
7. J.A.Armstrong, N.Bloembergen, J.Ducuing, P.S.Pershan , Phys. Rev. **127**, 1918 (1962)
8. M. Born and E. Wolf , " Principles of Optics ", Pergamon Press , Fifth Ed. (1975).
9. A.Yariv, P.Yeh , " Optical Waves in Crystals" Ed. J.Wiley and Sons , 1984.
10. J.P. Dowling , C. M. Bowden - J. Of Modern Optics - **41**, 345-351 (1994).
11. M Centini. M.Scalora, C.Sibilia, M.Bertolotti, M.Bloemer, C.M. Bowden " to be submitted for publ.
12. L. Poladian, Optics Letters **22**, 1571 (1997).
13. J.P. Dowling, In press. On IEEE Proceeding on Optoelectronics
14. J.W Haus, R.Viswanathan, M.Scalora, A.G.Kalocsai, J.D. Cole, J.Theimer , Phys.Rev.A **57**, 2120 (1998).

II. TRUE TIME DELAY DEVICE

(a) Introduction

From a technological standpoint, a fundamental need exists for resonant structures that provide strongly enhanced interaction of light signals and material systems without distorting the signals. Most structures, however, tend to impose their own spectral and temporal features on the propagating pulse, and do not allow contemporaneous strong local enhancement and group velocity reductions, and distortion-free transmission of the pulse. Therefore, we use recent advances in the understanding of pulse propagation and dynamics in one-dimensional PBG structures to explore the novel capabilities offered by these structures. Instead of working under the usual conditions where incident pulses may be short compared to the resonator dimensions, we use conditions where the pulse is long compared to the resonator's length. In essence, the pulse includes the resonator, rather than the other way around.

The consequences of this combination can be far reaching. While most of the pulse can be found in the surrounding space at any given time, the portion of the pulse located inside the structure experiences a significant reduction of group velocity by several orders of magnitude below the velocity of light in vacuum. Thus, despite the nature of the very strong interaction, the resonant process only appears to weakly perturb the pulse properties, other than to impose a large group delay.

In this study, we treat pulse propagation and dynamics in photonic crystals within the context of a small number of periods and large index contrast between layers ($\delta n = 0.4$ or greater). The pulse group velocity displays a $1/N^2$ dependence near the band edge, and $1/(N^2 e^N)$ for a Fabry-Perot defect cavity mode, where N is the number of periods [9]. Doubling the number of periods reduces the group velocity by a factor of 4 near the band edge, but also reduces the bandwidth of the first transmission resonance by the same factor. This effect is more pronounced at the defect mode because of the dependence on the exponential factor. It is thus desirable to increase the number of layers up to the point where the bandwidth has decreased to the order of pulse bandwidth.

(b) Review of Band Edge Delay Line

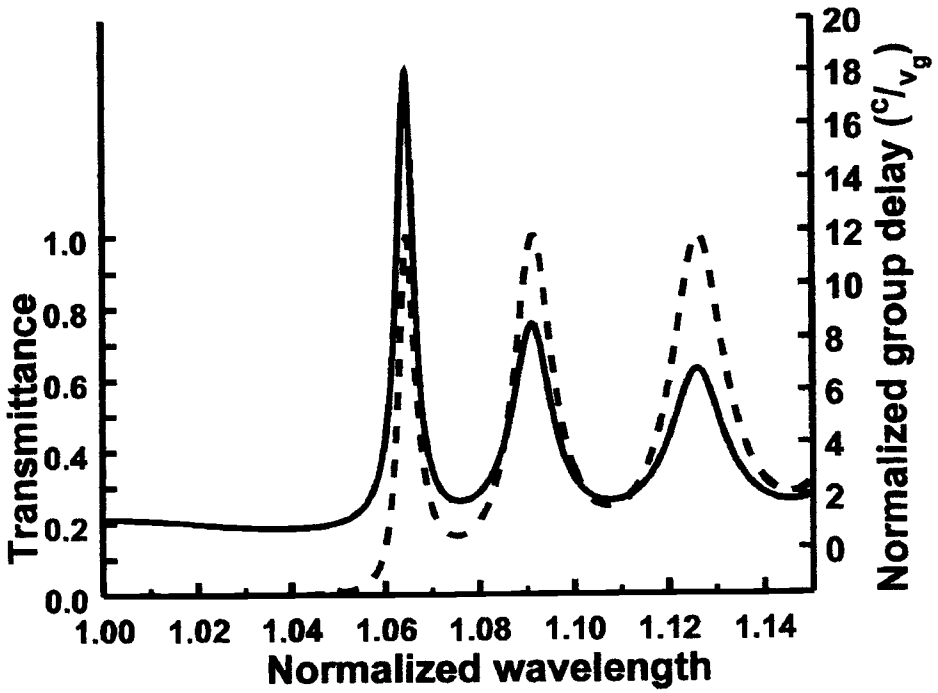

Figure 1

Recently, it has been shown that for a compact 8-micron thick structure one can achieve large reductions in group velocity for bandwidths that allow ultrashort optical pulse propagation [10]. This behavior is illustrated by the transmission curves for a 30-period quarter-wave stack of indices approximately 3.4 (GaAs) and 2.9 (AlAs) in Figure 1. The transmission (dashed line, left axis scale) is plotted as a function of the wavelength. Changes can be even more dramatic for a different set of indices. One can in principle use any combination of refractive indices, with an appropriate number of periods, to obtain an equivalent response. The solid line (right axis scale) represents the group index dependence on wavelength. Note that these functions oscillate in phase and are strongly correlated. The figure suggests that while overall transmission should be high, near the band edge pulses should propagate at a significantly reduced group velocity, about c/18 in this case.

Utilizing some recently developed calculational tools [11], we first performed simulations of the Maxwellís equation that describe pulse propagation in the simple one-dimensional structure. To obtain the density of states and the group velocity we used novel analytical and numerical methods. At the band edge, an ultrashort pulse can be transmitted with almost negligible degradation. In Figure 2, shows the spectrum of the 2-picosecond pulse that we use in our simulations (dotted line), and compare its spectral width to the bandwidth of the first transmission resonance (dashed line).
Note that the group velocity (solid line) is a minimum where the transmission is a maximum.

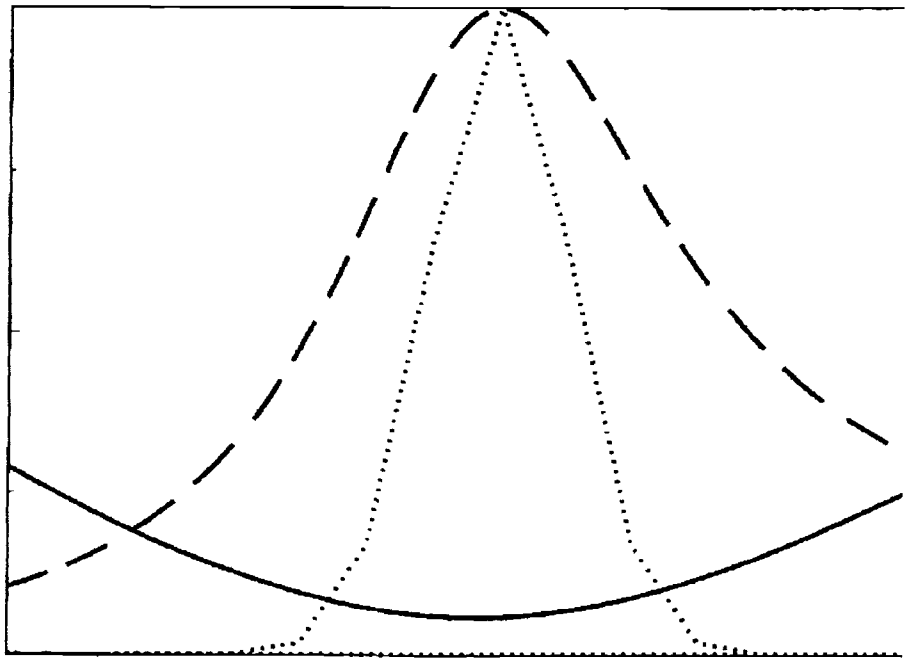

Figure 2 Picosecond Pulse

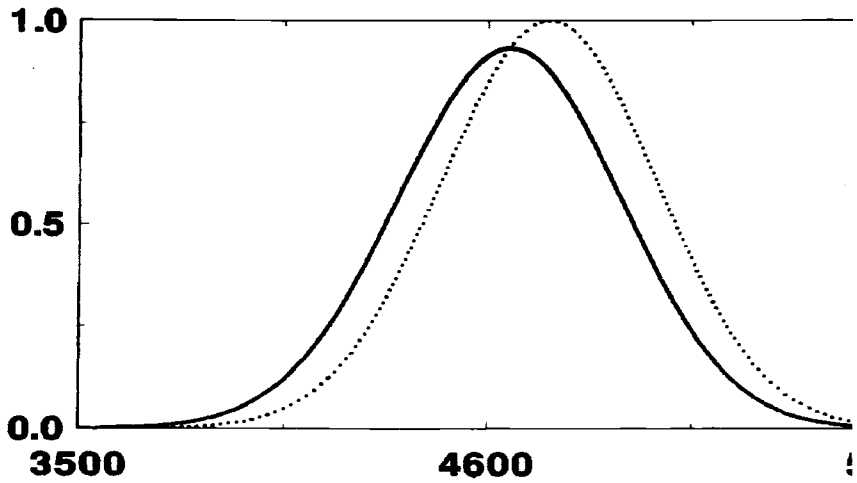

Figure 3

In Figure 3, the solid line is the result of a simulation where a pulse whose full width at half maximum is nearly 2 picoseconds (the carrier wavelength is 1.529 microns) propagates at the band edge; the dashed line represents the same pulse propagating in

vacuum. The longitudinal coordinate is scaled in nanometers. The results are that (a) the transmission is 95% or more, (b) the transmitted pulse is undegraded, (c) reflections are kept to a minimum, and (d) the pulse is delayed approximately 110 microns.

In Figure 4, we show the calculated electric (solid line) and magnetic (dashed line) field profiles (or eigenmodes) inside the multilayer cavity.

We use the term quasi-standing wave to describe this feature. In essence, a transient standing wave is created; however, the net result is almost complete transmission of the optical energy. This remarkable phenomenon has highly desirable features for ultrafast devices, and must be distinguished from what is typically referred to as a defect mode, which resembles a Fabry-Perot transmission resonance. In fact, the very high cavity-Q that a defect mode exhibits does not posses the bandwidth necessary for ultrashort pulse propagation; however, the same qualitative results are expected for longer pulses, as long as the frequency bandwidth of the incident pulse matches that of the defect mode. A clear advantage of the defect mode cavity is that much larger delays are possible.

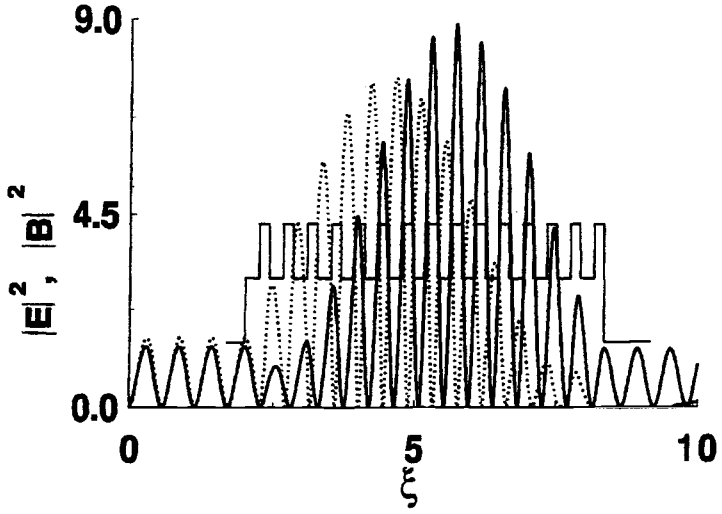

Figure 4 Calculated Electrical & Magnetic Field Profiles

Finally we note that the electric (magnetic) field is localized in the high (low) index layers; tuning the pulse to the high frequency band edge causes a shift in the localization to the low index layers. The reasons for this type of localization are similar to the properties of electron standing waves in crystalline structures. The electron tends

to concentrate near or in between the ion cores [12]. The difference in potential energy between these two electron distributions is equal to the energy gap. We do not wish to further exploit this analogy here, and simply note that in the case of photons, the Bloch phase of the field eigenmodes changes by π between the upper and lower band edges [9]. The qualitative aspects of the dynamics remain unaltered at both the high and low frequency band edges. The pulse undergoes multiple reflections inside the structure. The transmitted wave packet will be delayed by a time that is generally long compared to the single pass propagation time for the structure as compared to a pulse that propagates in vacuum, or a pulse tuned at a slightly different frequency.

An experiment was performed to verify the theoretical predictions described above, and the results have been previously reported in the open literature [10]; a patent application is pending on that device. For completeness, here we report the most salient results of that experiment. The sample consisted of a GaAs substrate, a 1.1166-micron thick spacer of AlAs, and a 30 period DBR stack of GaAs/AlAs. The optical thickness of each layer in the DBR stack is 1/4 of a wavelength for λ = 1446.6 nm. The total thickness of the 1-D photonic band gap structure, including the AlAs spacer, was 8 microns. An erbium-fiber laser provided 2-picosecond pulses at a 2-GHz rep-rate and a fixed center wavelength of 1529nm, where the low frequency band edge was located. Since the lasing wavelength was fixed, we measured the variation in the group velocity in the vicinity of the photonic band edge by examining the angular dependence of the group velocity. By simply rotating the sample, the laser can be tuned through the photonic band edge and into the photonic band gap. The maximum measured optical path through our structure plus AlAs spacer was 108 microns at an 18 degree angle of incidence. We illustrate this in Figure 5, where we plot the calculated (solid line) and measured (dots) optical delay as a function of incident angle. The pulse was transmitted through the photonic band gap medium with minimal distortion in pulse shape and a transmittance greater than 95%.

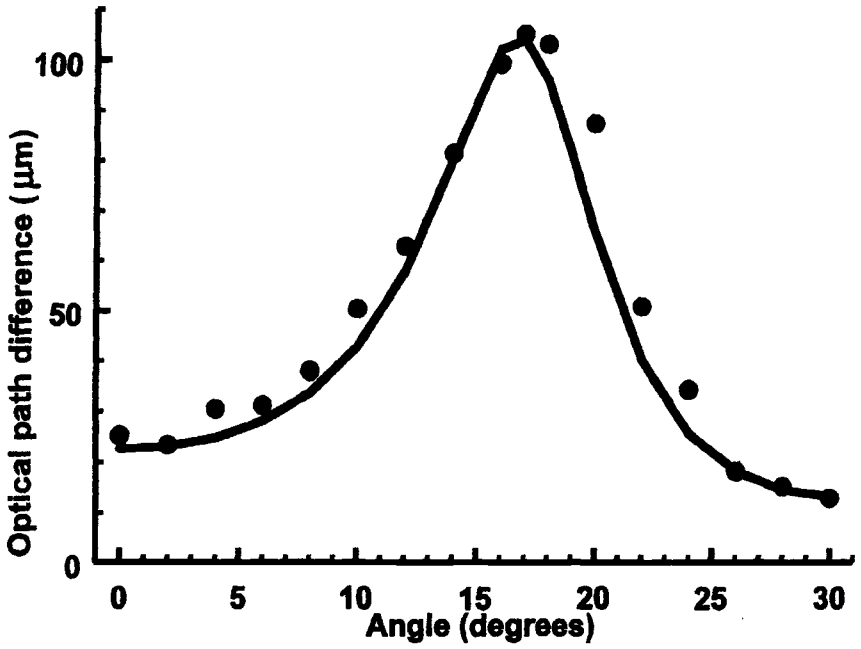

Figure 5 Calculated & Measured Optical Path

The measured group velocity data were compared to a theoretical model based on the matrix transfer method for multilayer films [13]. The calculated group velocity, $d\omega/dk$, was found to agree to within 5% of the measured values. This is completely consistent with the pulse propagation simulations, which indicate an increase in group velocity with respect to quasi-monochromatic wave trains by about 5% due to the finite pulse bandwidth, and is in excellent agreement with experimental results.

In view of our theoretical and experimental results, we note that a measure of the overall improvements over conventional technology can be gained by observing that commercial modulators, e.g., have bandwidths of order 10 GHz and require pathlengths of order ten centimeters to produce a group delay of approximately one optical wavelength. The resonator described here produces some 90 microns of adjustable group delay in only 8 microns of material. In terms of adjustable delay per unit distance, this is an improvement of some six orders of magnitude over conventional technology. Also in terms of bandwidth, there is an improvement of some two orders of magnitude, from 10 GHz to a terahertz. This gives an improvement in the product of delay per unit distance and bandwidth of some eight orders of magnitude. Considering the simplicity, compactness, tunability, and the apparent ability to iterate through several similar

structures with a proportional increase in delay, as we previously reported [10], these one-dimensional structures are truly remarkable. Exploitation of the physics of pulse propagation near the photonic band edge can lead to the next generation of a whole new class of ultrafast, highly compact, and cost efficient devices.

III. THE FABRY-PEROT DELAY LINE

As seen, the propagation of ultrashort pulses in one dimensional photonic band gap materials is characterized by strong interference effects that give rise to a gap in the transmitted spectrum of the incident light. The interference of backward and forward going waves can produce interesting effects near the photonic band edge. They include: order of magnitude enhancement of the electromagnetic mode density of states (or the number of photons per unit volume) and field magnitude; large delay of transmitted pulses; lossless and near unity transmission of the incident radiation.

Ultrashort pulse propagation near the photonic band edge, where these effects occur, has been studied by straight forward integration of Maxwell's equations of motion for the field envelopes in the slowly varying envelope approximation in time [2-11]. Using the approach outlined in Refs.(2-11), the theoretical prediction and the experimental verification of a linear, compact delay element soon followed [10]. To summarize, a 2-picosecond pulse was transmitted without loss, and delayed approximately 108 microns by a structure 8 microns in length, making the delay-to-device length ratio larger than one order of magnitude. The objective of the present study is to obtain delays on the order of 100 picoseconds, or approximately 30000 microns, with a device that is similar in nature and in length to the structure outlined in Ref.(10). That is, a layered, periodic, semiconductor structure only a few microns in length.

The 100-picosecond delay could be achieved with a structure similar to the one used in the experimental verification of the delay line for ultrashort pulses. The design consists of two quarter-wave stacks, each with 30 periods of GaAs/AlAS alternating layers, separated by a half-wave GaAs layer, such that the structure is symmetric for right and left propagating waves. (For simplicity, we do not include for the moment a substrate layer and material dispersion, although their incorporation in the model is simple; their inclusion does not change the qualitative results.) This configuration causes a sharp transmission resonance, often referred to as a "defect mode", or a Fabry-Perot resonance, in the middle of the photonic band gap. The properties of this transmission

resonance inside the gap are similar to the properties of the photonic band edge resonances. However, one crucial difference consists of the fact that the density of electromagnetic field modes (also a measure of group index, and hence group delay) is much larger for the defect mode (in excess of two orders of magnitude) than any band edge transmission resonance that can be obtained with the same total number of periods. The expected delays are therefore correspondgly higher by two orders of magnitude, for pulses that are about 100 ps in duration. We point out that Fabry-Perot cavities are routinely used in work were high-Q cavities are needed, such as in microcavity lasers systems. However, their use as true time delay elements is completely novel to our knowledge.

(a) Mathematical Formalism

We now briefly outline the mathematical procedure that used to calculate the transmissive properties - and most importantly, the group index - of the structure that we propose. The transmission function is a complex number that depends on frequency (or wavelength), and it can be easily calculated by using an ordinary matrix-transfer method for the propagation of single frequency components inside the layered structure [13]. We can define the transmission as,

$$T(\omega) = x(\omega) + i\,y(\omega) = |T| \exp[\,ik(\omega)L], \quad (1)$$

where $k(\omega)$ is the "effective" wave vector, L is the physical length of the structure, and $k(\omega)L$ is the total phase shift imparted to the transmitted field at frequency ω. Similar arguments can be made for the reflected portion of the field.

It follows that the dispersion relation, or more simply, the wave vector dependence on frequency, is given by,

$$\tan(k(\omega)L) = y(\omega)/x(\omega). \quad (2)$$

Simple differentiation of this expression then leads to [6],

$$dk/d\omega = (1/L)\,[y'x - yx']/[x^2+y^2], \quad (3)$$

where the ' symbol means differentiation with respect to ω. Eq.(3), which was first derived in Ref.(9), is simple, but fundamental. In fact, $dk/d\omega$ represents the density of states in units of C, the speed of light in vacuum. It is a direct measure of the group index, N_g, since $V_g = d\omega/dk = C/N_g$. Therefore, once the transmission $T(\omega)$ is obtained, group index and group delay easily follow. A light pulse will cross a sample of thickness L and index N_g in a time $\tau_d = L/V_g$. If the device were not in the path of the beam, the

time of flight would simply be $\tau_0 = L/C$. The net delay is therefore the difference between these two times of flight, that is, $\delta = \tau_d - \tau_0 = (N_g - 1)L/C$.

The formalism described above was used to predict the delay that was eventually shown to occur in the 30-period device analyzed in Ref.(10). There are at least two ways to undertake the study of pulse propagation: first, straight forward integration of Maxwell's equations of motion in the time domain [1-4]. This method is powerful, but it is best suited to study nonlinear dynamics of ultrashort pulses. An alternative method is based on the matrix transfer method. This method is considerably simpler, and utilizes symmetry and superposition principles to great savings in computational time. However, it can only be used in the linear regime, which will always be the case in what follows.

Generally, the transmission is defined as the ratio of the transmitted to incident field [13], that is,

$$T(\omega) = E_{out}(\omega) / E_{in}(\omega). \quad (4)$$

Therefore,

$$E_{out}(\omega) = T(\omega)\, E_{in}(\omega). \quad (5)$$

The function $T(\omega)$ can be viewed as a propagator that is calculated using the matrix transfer method. We multiply both sides of Eq.(5) by $\exp(-i\omega t)\, d\omega$, and integrate over all frequencies, i.e., take the Fourier Transform. The result is,

$$E_{out}(t) = \int_{-\infty}^{+\infty} T(\omega)\, E_{in}(\omega) \exp(-i\omega t)\, d\omega \quad (6)$$

where $E_{out}(t)$ is the temporal profile of the transmitted field. This is a simple procedure that allows calculation of the transmitted field in a straight forward, economical manner, and that correctly reproduces the results of Ref.(10). However, we emphasize that this method is applicable if medium response is linear, i.e., the index of refraction cannot be intensity dependent. The simple steps that must be followed are: first, the transmission function $T(\omega)$ is calculated for the structure; second, a function $E_{in}(\omega)$ is assumed; it can be completely arbitrary to the extent that it accurately reflects the temporal evolution and duration of the incident pulse; finally, the inverse Fourier

Transform of the product T (ω) E_{in} (ω) is calculated. The objective was to design and build a sample that was about 10-15 microns in length, with a delay of 100 picosecond per pass. However, such a structure requires a transmission resonance whose bandwidth is of order 0.02 nanometers, and contains a total of about 120 alternating GaAs/AlAs layers. However, current state of the art, molecular beam epitaxy (MBE) techniques do not allow fabrication of this sample to such a high degree of precision. This structure is quite thick, and any imperfection in surface smoothness at any interface inside the sample can cause large scattering losses (propagation away form the propagation axis), leading to little or no longitudinal transmission of the incident light.

The concept remains viable using different materials. For example, our calculations indicate that a 10-period, 3-micron long structure composed of Magnesium Fluoride (MgF_2, n = 1.37) and Germanium (Ge, n=4.2), with a one-wavelength thick Ge layer embedded inside it, can generate about 100 picoseconds of delay if the incident pulse has a carrier wavelength at about 2 microns, where absorption is negligible. This is the same delay as the 60-period, GaAs/AlAs device that we had originally proposed. However, because we only assume a device 10-periods long, scattering losses should not be an important factor. The reason one needs fewer periods in this case is due to the fact that the index modulation depth, $\delta n = |n_2 - n_1|$, is now of order 3, while it was of order 0.4 in the case of GaAs and AlAs. The delay is in fact a sensitive function of the index modulation depth. We intend to pursue this new design in the development of a Phase II project with Time Domain Corporation (TDC).

Nevertheless, we determined that a viable GaAs/AlAs structure could still be fabricated using MBE techniques, in order to show a delay of about 10 picoseconds. The structure consists of two quarter-wave stacks (this condition occurs when λ = 1560 nm), one with 22 periods, and the other with 18 periods of GaAs/AlAs alternating layers, separated by a one-wavelength GaAs layer, to form an asymmetric structure. This entire structure is then grown on a GaAs substrate. We schematically depict this device in Figure 6. This configuration creates a sharp transmission resonance with a full width at half maximum of approximately $\delta\lambda$ = 0.34 nm in the middle of the photonic band gap, at λ = 1560, and maximizes the transmission to unity. The properties of this transmission resonance inside the gap are similar to the properties of the photonic band edge resonances, except for the location of the transmission resonance, and the magnitude of the group index for this

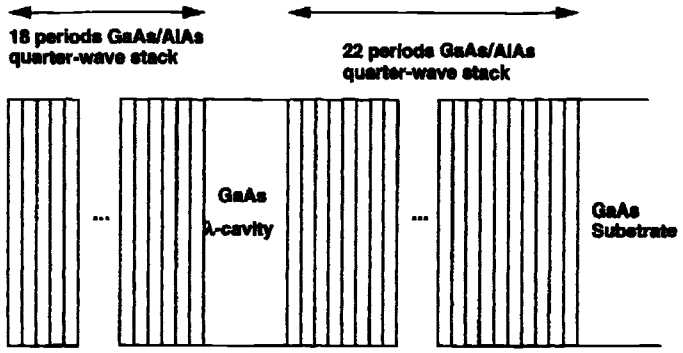

Figure 6) GaAs/AlAs Structure Schematic

defect mode which is about two orders of magnitude larger than the group index of the band edge delay line that we discussed above.

In Figure 7, we plot the calculated transmission ($|T|^2$) of the Fabry-Perot, photonic band gap. For this structure, we calculate the maximum group index to be about N_g=223. Due to the limited bandwidth, this means that any pulse tuned at the resonance maximum, and whose duration is greater than about 50 ps will propagate at the group velocity of C/223. The physical length of the structure is approximately L=10.3 microns; taking C=3x10^8 m/sec., the delay is then approximately δ=8 picoseconds; this delay is one order of magnitude smaller compared to what we originally sought.

Although 8 ps is not as ambitious as 100 ps, the delay-to-device length (now 40 periods) ratio is approximately 2400, still a remarkable ratio, considering the structure is only 10 microns in length, and two to three orders of magnitude larger than is currently achievable by any other means! We now invoke the other major result of the experiment of Ref.(10) that we alluded to earlier: the total delay was found to be proportional to the number of structures traversed by the pulse, or proportional to the number of passes through a single PBG sample. This means that if the sample can be introduced in a simple cavity configuration, such that the beam is made to traverse the sample several times, a tunable 100 ps delay could be achieved.

Therefore, our current optimum sample consists of a 40 period, GaAs/AlAs structure, with a one-half wavelength GaAs layer, as shown on Figure 6. The predicted

group delay for a pulse whose duration exceeds 50 ps, tuned at the Fabry-Perot resonance, is approximately 8 picoseconds.

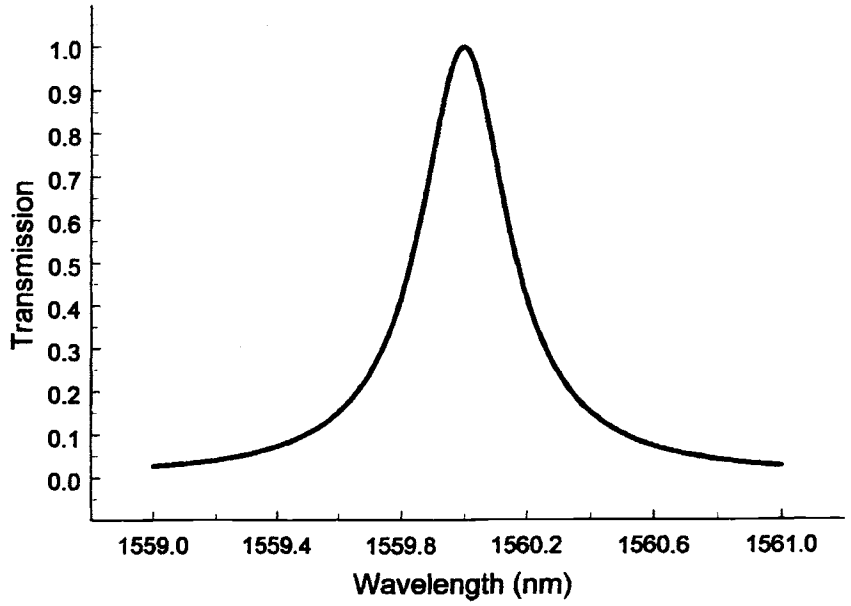

Figure 7 Calculated Transmission

Device Fabrication

A sample, similar to the one depicted in Figure 6, was fabricated using MBE techniques at the Univeristy of Arizona by the group led by Prof. Hyatt Gibbs, under a JSOP agreement. In Figure 8, the percentage of light transmitted is shown as a function of a broad range of incident wavelengths. We note the appearance of the transmission resonance in the middle of gap, at $\lambda = 1550$. Due to thickness variations across the sample, we expected and found that the band structure can shift up or down in wavelength by as much as 20 nm. However, all qualitative aspects of the transmission function are preserved.

In Figure 9, we show the details of the transmission resonance. The maximum transmission is about 61%. Refering now refer to Figure 6, the transmission into the substrate from the PBG structure is nearly unity, as predicted by our theoretical model. The reason the transmission drops to 61% upon exciting from the substrate into air is

because of the index discontinuity present between the substrate (n=3.4) and the background medium, in this case air (n=1). If we account for this in our model, then the transmission from the device, which includes the substrate-air interface, is approximately 61%; the rest is lost to reflections from the substrate-air interface. However, this drop in transmission does not affect the group velocity inside the PBG device, since the PBG and the substrate-air interface are spatially separated by the substrate thickness.

Our model predicted a full width at half-maximum (FWHM) of approximately 0.34 nm for the Fabry-Perot transmission resonance, with a maximum delay of about 8 ps at the transmission maximum. On the other hand, the sample displays a slightly broader FWHM of 0.37 nm, and some structure near the transmission maximum which suggest a slightly narrower peak. This may be due to uncertainties that arise during fabrication; however, the sample is more than suitable for our purposes.

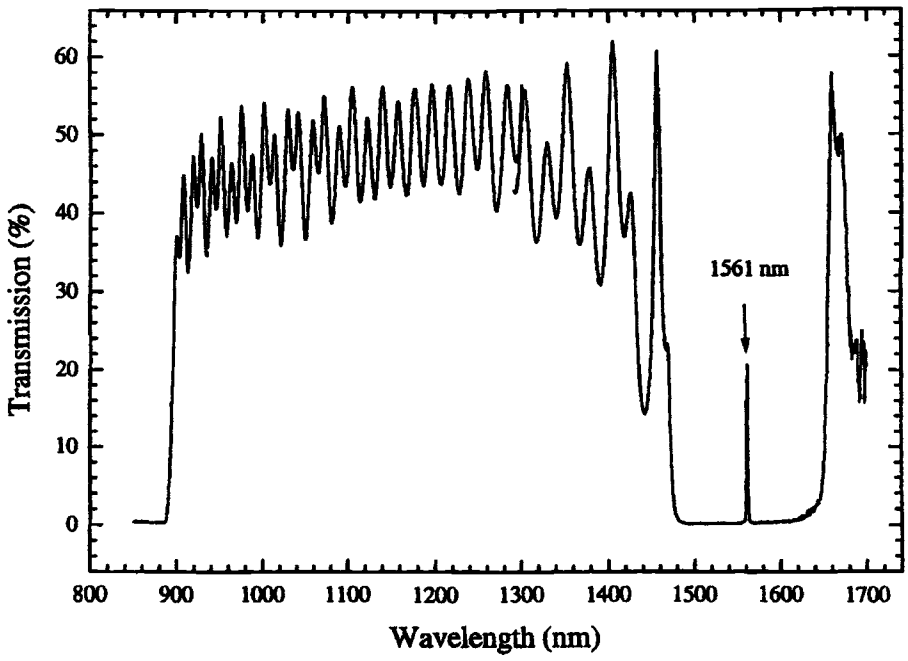

Figure 8 – Percentage of Light Transmission

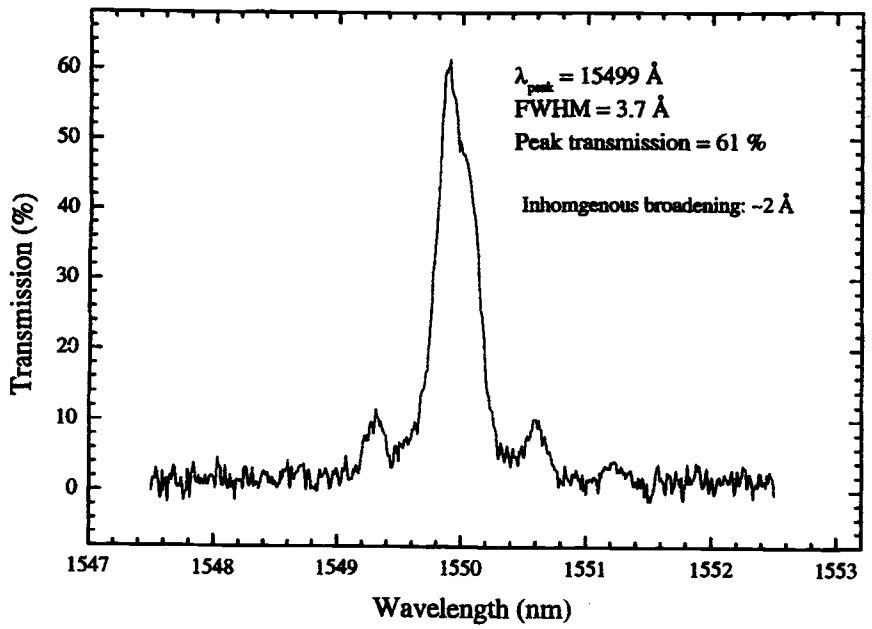

Figure 9- Transmission Resonance

Experimental Test

The predicted magnitude of the delay was large enough that it was detectable using a high-precision oscilloscope configured to measure pulse delays.

The laser pulses were generated with a New Focus, extreme-stability tunable diode laser, centered at 1549nm. This laser can be amplitude-modulated using an SMA input on the laser head that is connected directly to the diode. An Avtec AVM-1-C-DSRCA pulse generator was driving the modulation input, with 0.5 volt / 2ns pulses. The diode output was passed through a variable attenuator so that the power on the detector could be tuned to a constant level, no matter how the sample was tuned. This eliminated possible biasing of the diode response, which could change with different power levels. The beam was first directed through the attenuator; it was then focused onto the sample with a 3x objective. A second objective on the opposite side of the sample was used to focus the beam onto the detector.

The sample was mounted on a linear translator so that a micrometer could be used to tune across the Fabry-Perot transmission resonance. The detector used was a New Focus-1611, 1-GHz photoreceiver. Its rise time is 400ps, which is sufficient for use with the modulated laser rise time of 700ps. The DC level of the detector and the room temperature were both monitored with a digital multimeter. The AC component of the detector was hooked to an HP-54121, 20-GHz sampling scope; this was accurate enough to measure the rise time of the laser and detector. In order to accurately determine the position of the peak of the pulse in time, we sampled twenty thousand data points; the scope was then used to perform a statistical analysis of the data. The scope was triggered from the output of the pulse generator; the time from trigger to detector output was then measured. The accuracy of this setup without the sample was shown to be approximately 1ps. Since our predicted delay was on the order of 8 ps, this setup therefore was shown to have both the stability and accuracy necessary to perform the measurement.

Calibration data was first taken so that we could correct for temperature drifts in the equipment. Once this was done, we took three different data sets using the sample, and one data set on a known glass sample that we used as a reference. The delay from the glass sample was calculated, from known thickness and index of refraction, to be about 10ps. In this case, we measured a delay of 9.91ps, in good agreement with the prediction. This gave us enough confidence in our equipment and methods, and at this point we inserted the PBG sample in the path of the beam.

We first tuned the beam at wavelengths where the transmission, and the delay, are a minimum. There was no measurable delay in the transmitted pulse, as expected. To record the maximum delay, we took three sets of data; in each case, the measured delays were 13ps; 10.6ps; and 10.8ps respectively. Allowing for an uncertanty of approximately 1ps due to the accuracy of our equipment, all these measurements indicated a delay that was indeed of order 10 picoseconds, but slightly greater than our original prediction of 8 picoseconds.

As pointed out earlier, this small discrepancy may be due to the structure present in the transmission resonance, e.g. a slightly narrower peak that the sample in reality displays. Recall that narrower transmission resonances are associated with higher cavity-Qs, and therefore higher delays. We believe that this explains the slight deviations from our theoretical predictions; we cannot say, however, where inside the sample we may

find the imperfections that give rise to the complex structure in the peak of the transmission resonsance.

The measurement process was complicated by the fact when the sample was tuned away from its peak transmission, very small fluctuations could cause large shifts in transmission and delay, probably due to the large slope of the transmission curve in that wavelength range. This made it difficult to maintain the system stable while tuned off peak. On the other hand, tuning to the wavelength where peak transmission occurred caused much smaller fluctuations, minimizing jitter in the diode signal, and giving a very stable measurement. If the sample was tuned far enough away from the transmission peak, we found that the signal became stable again; however, the signal strength was much smaller because the transmission was lower.

For sample sets 2 and 3 (10.6ps and 10.8ps respectively), the variation in the DC voltage measured was stable, and less than 10mv, giving us reason to believe that both of these data sets are accurate. On the other hand, sample set 1 (13ps) was not as stable, having a voltage variation of about 45mv, and its validity is in doubt.

4.0 CONCLUSION

We have theoretically predicted, and experimentally demonstrated, that a delay line based on photonic band gap structures is indeed feasable for integrated circuit applications. Although our original goal of 100ps per pass had to be scaled back to 10ps per pass due to limitations in current fabrication technique, we believe that it is currently possible to obtain 100ps per pass and beyond, using different materials and compound structures. We also recognize that a delay of 10ps that we obtained from the current device can be extremely useful for immediate applications to systems that utilize optical control of microwave phased array radars, where even more modest delays are generally sought. This field is currently in need of the type of breakthrough technology that the photonic band gap delay line represents, that we have demonstrated.

REFERENCES

[1] E. Yablonovitch, Phys. Rev. Lett. **58**, 2169 (1987).

[2] Development and Applications of Photonic Band Gap Materials, edited by C. M. Bowden, J. P. Dowling, and H. O. Everitt, J. Opt. Soc. Am. B **10** , 279-413 (1993), special issue; also G. Kurizki and J. W. Haus eds., J. Mod. Opt. **41** (1994) , special issue.

[3] J.P. Dowling, M. Scalora, M.J. Bloemer, and C.M. Bowden, J. Appl. Phys. **75**, 1896 (1994).

[4] M. Scalora, J.P. Dowling, M.D. Tocci, M.J. Bloemer, C.M. Bowden, and J.W. Haus, Applied Physics B **60**, S57 (1995); J.P. Dowling and C.M. Bowden, Phys. Rev. A **46**, 612 (1992).

[5] M. Scalora, J. P. Dowling, C. M. Bowden, and M. J. Bloemer, Phys. Rev. Lett. **73**, 1368 (1994).

[6] M. Scalora, J. P. Dowling, C. M. Bowden, and M. J. Bloemer, J. Appl. Phys. **76**, (1994).

[7] M.D. Tocci, M.J. Bloemer, M. Scalora, J.P. Dowling, and C.M. Bowden, J. Appl. Phys. **66**, 2324 (1995).

[8] M.D. Tocci, M. Scalora, M.J. Bloemer, C.M. Bowden, and J.P Dowling, Phys. Rev. A **53**, 2799 (1996).

[9] J.M. Bendickson, J.P. Dowling, and M. Scalora, Phys. Rev. E **53**, 4107 (1996).

[10] M. Scalora, R. J. Flynn, S. B. Reinhardt, R. L. Fork, M. J. Bloemer, M. D. Tocci, J. Bendickson, H. Ledbetter, C. M. Bowden, J. P. Dowling, and R. P. Leavitt, Phys. Rev. E **54**, 2799 (1996).

[11] M. Scalora and M.E. Crenshaw, Opt. Commun. **108**, 191 (1994); J.B. Cole, R.A. Krutar, S.K. Numrich, and D. Creamer, Computers in Physics **9**, 235 (1995); H. Ledbetter, 1995 Technical Report for DOD Science and Engineering Apprentice Program.

[12] C. Kittel, Introduction to Solid State Physics, 5th edition, pp. 188-189, (John Wiley and Sons, New York, 1976).

[13] G. R. Fowles, *Introduction to Modern Optics,* Dover Publications Inc., New York, 1968, 1975, Chapter 4.